https://doi.org/10.1016/j.engstruct.2018.07.010

Thermal Effect on Vibration and Buckling Analysis of Thin Isotropic/Orthotropic Rectangular Plates with Crack Defects

S.K. Lai[a,b,*] and **L.H. Zhang**[a]

[a] *Department of Civil and Environmental Engineering, The Hong Kong Polytechnic University, Hung Hom, Kowloon, Hong Kong, P.R. China*

[b] *The Hong Kong Polytechnic University Shenzhen Research Institute, Shenzhen, P.R. China*

Abstract

The present research is concerned with the vibration analysis of thin isotropic and orthotropic rectangular plates with crack defects under thermal environmental conditions. In the literature, there are only few studies reported in this direction. Based on the classical plate theory, the governing equations of the isotropic and orthotropic cracked rectangular plates can be derived, in which a surface crack located at the plate center is formulated based on a line-spring model. Since the dynamic behavior of structural elements is significantly affected by thermal effects, a thermal buckling analysis for isotropic and orthotropic plates is also conducted. A uniform heating load on the cracked rectangular plates is considered and the critical buckling temperature of the plates with or without cracks is investigated. The discrete singular convolution (DSC) method is then applied to formulate the eigenvalue equations for the cracked rectangular plates under various thermal conditions. The DSC technique is an ingenious method in stability and dynamic analysis of plates, not only it is a flexible local method to handle complex geometries and boundary conditions, but also it performs as a global approach with a high degree of accuracy. To go beyond the limitation of the DSC method, the use of Taylor's series expansion method is incorporated for the treatment of free boundary conditions. In addition, this is the first attempt to explore its application on the analysis of cracked rectangular plates under

*Corresponding author.
Tel.: (852) 2766 6060; Fax: (852) 2334 6389; E-mail address: sk.lai@polyu.edu.hk

thermal effects. In this work, the vibration of isotropic and orthotropic cracked rectangular plates with various combinations of boundary conditions is studied. A special restrained manner of simply supported conditions that are permissible for in-plane movements is also analyzed. The obtained solutions herein are compared with the existing results to verify the accuracy and reliability. Besides, accurate first-known solutions are also presented.

Keywords: Thermal effect, Surface crack, Isotropic and orthotropic plates, DSC method.

1. Introduction

Thin-walled rectangular plate-type structures are basic elements in structural and mechanical engineering. Although the dynamic and buckling behavior of thin plates have received great attention, many modern structures are made of composite materials due to their high strength-to-weight and stiffness-to-weight ratios. Composite materials can be generally modeled as orthotropic plates. The orthotropic properties are obtained by changing the isotropic characteristics along perpendicular directions and utilizing anisotropic materials during manufacturing processes. From a perspective view of mechanics, thin isotropic and orthotropic plates are often subject to various in-plane forces and moments by strong dynamic loads. A long-term influence from dynamic responses is to induce potential damages on such plates, resulting in the failure of structures. Therefore, the detection and localization of damages or cracks to thin isotropic and orthotropic plates are crucial for the safety requirement and good performance in their service life. Besides, the exposure of thin isotropic and orthotropic plates in thermal environments would affect the plate stiffness and change its dynamic behavior. Motivated by the need to address this issue, the understanding of the dynamic and stability analysis of cracked isotropic and orthotropic plates subject to thermal conditions is highly desired.

In the early scientific monographs [1-4], the dynamic characteristics of various structural elements have been intensively studied. The fundamental theories have been well established to provide useful guidelines for structural design and control. Stability and vibration studies for cracked thin plates have been developed in the past decades. Wang *et al.* [5] provided generic buckling solutions for Mindlin plates of various shapes, including polygonal, elliptical, semicircular and annular plates. For beam structures, Feng *et al.* [6] recently presented an investigation on the nonlinear free vibration of a multi-layer polymer nanocomposite beam reinforced by graphene platelets. On the other hand, many scholars have devoted to the investigation of crack effects on plates, involving part-through surface cracks, part-through finite length

cracks, all part-through cracks and internal cracks [7-11]. For instance, Rice and Levy [7] introduced a line-spring model (LSM) based on the classical Kirchhoff plate theory to evaluate the effect of plate cracks. In their work, the part-through crack is represented by a continuously distributed line-spring. The appropriate compliance coefficients were chosen to match the tension and bending of an edge-cracked tip in terms of plane strains. Furthermore, Israr *et al.* [12] proposed an analytical model for isotropic rectangular plates with cracks using the LSM. According to the work from Aksel and Erdogan [13], they considered the stress intensity factor to account for internal cracks and established the crack compliance coefficients using a set of polynomial functions. Moreover, Joshi *et al.* [14] constructed an analytical model for the vibration analysis of internally cracked rectangular plates using the LSM, in which the compliance coefficients are variances with the ratio of d/h (i.e., d is an offset distance between the crack center line and the neutral plane, and h is the plate thickness). Bose and Mohanty [15] extended the previous model [12] to investigate the dynamic characteristics of rectangular plates with an angled crack. They also took the effect of the far-field tensile stress on the crack tip bending stress into consideration.

In addition, there are research studies on the vibration of cracked plates by means of numerical techniques. Liew *et al.* [16] employed the domain decomposition method by utilizing appropriate shape functions for cracked plates with typical boundary supports. Huang and Leissa [17] applied the Ritz method combined with various composition techniques to investigate the effects of crack location, crack length and orientation on the vibration of plates. Xu and Chen [18] used the differential quadrature finite element method to study the dynamic behavior of plates with irregular shaped cracks.

As aforementioned, composite material structures can be simplified as orthotropic plates. Many relevant research studies on orthotropic plates have been conducted. Xing and Liu [19] applied a separation of variables to obtain exact solutions for the free vibration of thin orthotropic plates. Biancolini *et al.* [20] investigated the approximate

evaluation for the vibration frequencies of orthotropic plates. In their work, a particular form of the Rayleigh method was used to simplify the calculation procedures. Kurpa *et al.* [21] studied the free flexural vibration of thin orthotropic plates with mixed boundary conditions by the method of R-function. On the other hand, Joshi *et al.* [22] extended the analytical model developed by Israr *et al.* [12] to thin rectangular orthotropic plates with crack defects. They discussed the effects of crack length and boundary condition on the natural frequency of such plates. Yum and Hong [23] analyzed the mixed mode fracture problem for finite orthotropic plates with an inclined crack. Szekrényes [24] incorporated the classical laminated and first-order shear deformable plate theories to construct a double-plate system for the analysis of delaminated orthotropic composite plates. Shen *et al.* [25] utilized the Rayleigh-Ritz method to investigate the bending and vibration characteristics of a strengthened plate under various boundary conditions.

It is commonly known that engineering structures are usually exposed in thermal environment during their service life. The dynamic and stability behaviors of plate structures can be adversely affected by thermal conditions. In an early effort, Jadeja and Loo [26] investigated the thermally induced vibration of rectangular plates with one edge clamped and all other edges simply supported. They applied the Galerkin method to obtain the deflection curve of the plates. Shen [27] analyzed the thermal post-buckling behavior of imperfect shear deformation laminated plates. The thermal loads can be produced as a uniform temperature rises. More recently, Zhou *et al.* [28] used the Hamilton principle to derive the governing equation of motion for orthotropic plates under thermal conditions. In their work, the acoustic radiation effect of orthotropic plates was also discussed. Indeed, the formation of cracks can seriously affect the intrinsic property of structure elements, inducing the loss of stability. Hence, the understanding of vibration characteristics of cracked rectangular plates in thermal environment is another crucial topic. In the literature, only a limited number of studies have reported for the vibration analysis of cracked rectangular plates under thermal

effects. Sahin *et al.* [29] applied the finite element method to investigate the thermal buckling behavior of anti-symmetric composite square plates. Natarajan *et al.* [30] presented a study for the free vibration of cracked functionally graded plates under thermal effects. They discussed the influence of various parameters, including crack length, aspect ratio, temperature effect and boundary condition, on functionally graded plates. Rahimabadi *et al.* [31] studied the thermal effect on the vibration of functionally graded material plates with the presence of a centrally located circular crack. In addition, Joshi *et al.* [32, 33] proposed analytical models for the vibration analysis of cracked thin rectangular plates under thermal effects.

The present research focuses on the vibration and buckling analysis of isotropic and orthotropic thin rectangular plates with crack defects in thermal environment, it aims to develop an accurate and efficient solution for the prediction of structural responses by using the discrete singular convolution (DSC) method. This numerical approach was originally proposed by Wei [34, 35] for solving the Fokker-Planck equation. According to the previous works [36, 37], the DSC method is more stable than the differential quadrature method in the prediction of thousands of vibration modes of beams and plates. Although the DSC method is regarded as a local spectral method to possess the ability for handling complex geometries and boundary conditions, it also performs as a global numerical method with a high level of accuracy [38]. Wei *et al.* [39] firstly utilized the DSC method to analyze plate structures with internal supports. Lai *et al.* [40, 41] employed the DSC method for solving buckling and vibration problems of transversely supported and standing vertical rectangular plates. To extend the applicability of the DSC method, the DSC-Ritz method was proposed for analyzing the vibration of thick plates and shallow shells [42-44]. Civalek [45-48] further explored the DSC approach for solving a variety of laminated shell and plate problems. Wang and his colleagues [49-54] provided plentiful research works using the DSC method for various structure problems, e.g., multiple-stepped beams. On the basis of the DSC approach, Xiang *et al.* [55, 56] also developed the DSC-Element

method to investigate the dynamic characteristics of Mindlin plates with mixed edge supports and skew angles. Since the original version of the DSC approach is restricted for dealing with vibration and buckling analysis of plates with free edges, Wang *et al.* [56, 57] incorporated the DSC method with the Taylor series expansion technique to pass through this bottleneck.

Although there are many merits of the DSC method, to the best of the authors' knowledge, the DSC method has not been applied to investigate the vibration analysis of isotropic and orthotropic plates with crack defects in thermal environment. This research offers a comprehensive study for the vibration and buckling analysis of cracked plates under various boundary and thermal conditions. A special restrained manner of simply supported conditions that are permissible for in-plane movements under thermal conditions is also investigated. To go beyond the limitation of the original DSC approach, the Taylor series expansion method [57, 58] is incorporated to address the free vibration problem of plates with free boundary constraints. To formulate an eigenvalue problem, a small matrix-band of the DSC method is employed herein. This can also enhance the computational effort in dealing with large-scale structural calculations. The results are compared with the available solutions to validate its accuracy and reliability. Besides, accurate first-known solutions are also presented in this paper.

2. Formulation of mathematical models

Consider a rectangular thin plate with length L_1 in the x-direction, width L_2 in the y-direction and uniform thickness h. As shown in Fig. 1, a continuous part-through crack parallel to the x-axis with a length of $2a$ is located at the plate center, and a part-through crack is along the y-axis with a length of $2b$ (i.e., the dashed line). For an orthotropic plate, the independent elastic constants, including Young's modulus (E_x, E_y), Poisson's ratio (ν_x, ν_y) and shear modulus (G_{xy}), are required for mathematical

formulation. In the context of an isotropic thin rectangular plate, the same values of Young's modulus (E) and Poisson's ratio (v) along the two directions can be used.

2.1. Governing equations

Based on the classical plate theory and the line-spring model, the governing equation of thin rectangular orthotropic plates with a surface part-through crack along the x-axis in thermal environment is written as follows [7, 12, 32, 33]

$$\begin{aligned} &D_x \frac{\partial^4 w}{\partial x^4} + 2B_o \frac{\partial^4 w}{\partial x^2 \partial y^2} + D_y \frac{\partial^4 w}{\partial y^4} \\ &= -\rho h \frac{\partial^2 w}{\partial t^2} - N_x^T \frac{\partial^2 w}{\partial x^2} - N_y^T \frac{\partial^2 w}{\partial y^2} - \frac{\partial^2 M_x^T}{\partial x^2} - \frac{\partial^2 M_y^T}{\partial y^2} + \frac{\partial^2 \bar{M}_y}{\partial y^2} + \bar{N}_y \frac{\partial^2 w}{\partial y^2} + P_z \end{aligned} \tag{1}$$

where w is the transverse displacement, ρ is the plate density, h is the plate thickness, t is time, $B_o = D_x v_y + G_{xy} h^3/6$, $D_x = E_x h^3/[12(1-v_x v_y)]$ and $D_y = E_y h^3/[12(1-v_x v_y)]$ are the flexural rigidities with E_x and E_y being Young's modulus and v_x and v_y being the Poisson's ratio in the x- and y-directions, respectively. In addition, N_x^T and N_y^T are the in-plane forces per unit length due to the thermal effect. M_x^T and M_y^T are the moments induced by non-uniform heating loads. $\bar{N}_y$ and $\bar{M}_y$ represent the in-plane force and moment resulted by the presence of a crack, respectively. P_z denotes the transverse load per unit area acting on the surface.

As the governing equation of isotropic plates is only a subset of the orthotropic one, we can express the following terms in Eq. (1) to obtain the isotropic equation.

$$E_x = E_y = E, \quad v_x = v_y = v \quad \text{and} \quad D_x = D_y = B_o = D \tag{2}$$

where $D = Eh^3/[12(1-v^2)]$ is the flexural rigidity with E and v being Young's modulus and the Poisson's ratio, respectively.

2.2. Crack terms formulated by a line-spring model

To investigate the crack effect on the dynamic characteristics of plates, the LSM is used to formulate those crack terms in the governing equation. The LSM was proposed by Rice and Levy [7] based on the classical plate theory. They constructed an approximate relationship between the nominal tensile stress and the bending stress at the crack location and at the far sides of the cracked plate. Then, the relationship can be converted into a force effect, and the crack compliance coefficients are employed to represent the crack terms. Making use of the LSM, cracked plate models can be transformed into a two-dimensional problem, in which the variation of stress at the crack location with the change of the crack depth can be ignored. This releases the constraint of the three-dimensional nature in exact analysis. The uniformly distributed tensile stress σ_{rs} and the bending stress m_{rs} are assumed at the two sides of the crack location as illustrated in Fig. 2. The tensile stress and the bending stress at the far sides of the cracked plate can be written as [7, 12]

$$\sigma_{rs} = \frac{N_{rs}}{h} = \frac{1}{h}\int_{-h/2}^{h/2} \tau_{rs}(x,y,z)dz \tag{3}$$

$$m_{rs} = \frac{6}{h}M_{rs} = \frac{6}{h^2}\int_{-h/2}^{h/2} z\tau_{rs}(x,y,z)dz \tag{4}$$

where $\tau_{rs}(x,y,z)$ is the stress state, r and s are intermediate variables, N_{rs} and M_{rs} are the force and moment per unit length in the direction perpendicular to the crack length at the plate edge, respectively. Based on the LSM, a crack can be represented as a continuous line-spring having its compliance. These compliance coefficients are used to establish the relationship between the tensile stress and the bending stress at the far sides of the cracked plate and the crack location as follows

$$\overline{\sigma}_{rs} = \left[\frac{L_c}{(6\alpha_{tb}^o + \alpha_{tt}^o)(1-\nu^2)h + L_c}\right]\sigma_{rs} \tag{5}$$

$$\overline{m}_{rs} = \left[\frac{L_c}{3\left(\alpha_{bt}^o/6 + \alpha_{bb}^o\right)(3+\nu)(1-\nu)h + L_c}\right]m_{rs} \tag{6}$$

where L_c is the crack length, h is the plate thickness and v is Poisson's ratio. $\bar{\sigma}_{rs}$ and $\bar{m}_{rs}$ denote the nominal tensile stress and the bending stress at the crack location, respectively. Besides, α_{bb}^o, α_{tt}^o and $\alpha_{bt}^o (= \alpha_{tb}^o)$ denote the non-dimensional bending compliance coefficient, stretching compliance coefficient and stretching-bending compliance coefficient at the crack center, respectively.

According to the work of Israr *et al.* [12], Eqs. (5) and (6) can be written in terms of force and moment. They are added into the cracked plate model with a negative sign due to the reduction of the overall stiffness from damages. Without loss of generality, these two terms related to the crack are presented as

$$\bar{N} \equiv -\bar{N}_{rs} = -\left[\frac{L_c}{(6\alpha_{tb}^o + \alpha_{tt}^o)(1 - v_k{}^2)h + L_c} \right] N_{rs} \tag{7}$$

$$\bar{M} \equiv -\bar{M}_{rs} = -\left[\frac{L_c}{3(\alpha_{bt}^o/6 + \alpha_{bb}^o)(3 + v_k)(1 - v_k)h + L_c} \right] M_{rs} \tag{8}$$

Consider that there are cracks in two different directions as shown in Fig. 1, we have

$$L_c = 2a, \quad v_k = v_x \quad \text{and} \quad M_{rs} = -D_y \left(\frac{\partial^2 w}{\partial y^2} + v_x \frac{\partial^2 w}{\partial x^2} \right) \tag{9}$$

$$L_c = 2b, \quad v_k = v_y \quad \text{and} \quad M_{rs} = -D_x \left(v_y \frac{\partial^2 w}{\partial y^2} + \frac{\partial^2 w}{\partial x^2} \right) \tag{10}$$

where the flexural rigidities are $D_x = D_y = D$ and the Poisson's ratios become $v_x = v_y = v$ if the isotropic case is taken into consideration.

The compliance coefficients depend on the crack depth d and the plate thickness h. The three appropriate compliance coefficients in Eqs. (5) and (6) can be calculated by the following equations that are valid for the ratio $\zeta = d/h$ within the range 0.1 – 0.7 [7, 59, 60].

$$\begin{aligned} \alpha_{tt} = \zeta^2 (&1.98 - 0.54\zeta + 18.65\zeta^2 - 33.70\zeta^3 + 99.26\zeta^4 - 211.90\zeta^5 \\ &+436.84\zeta^6 - 460.48\zeta^7 + 289.98\zeta^8) \end{aligned} \tag{11}$$

$$\alpha_{bb} = \zeta^2(1.98 - 3.28\zeta + 14.43\zeta^2 - 31.26\zeta^3 + 63.56\zeta^4 - 103.36\zeta^5 + 147.52\zeta^6 - 127.69\zeta^7 + 61.50\zeta^8) \tag{12}$$

$$\alpha_{bt} = \alpha_{tb} = \zeta^2(1.98 - 1.91\zeta + 16.01\zeta^2 - 34.84\zeta^3 + 83.93\zeta^4 - 153.65\zeta^5 + 256.72\zeta^6 - 244.67\zeta^7 + 133.55\zeta^8) \tag{13}$$

The calculation results of the compliance coefficients for the center of the crack should take a proper non-dimensional procedure as

$$\alpha_{xy}^{o} = 1.1547\alpha_{xy} \tag{14}$$

where $x, y = b, t$ are intermediate variables for algebraic simplification.

2.3. Thermal effect on in-plane force and moment of thin plates

The analytical models of partially cracked plates presented above are proposed by Joshi *et al.* [32, 33]. This is an extended work of Israr *et al.* [12] based on the LSM. A stretching effect produced by the lateral deflection to cause non-linear motion is neglected. Only the membrane force due to the variation of temperature is considered in the LSM (i.e., $N^T = N_{rs}$). For an orthotropic plate under thermal conditions, the thermal stress parameters can be defined as [61]

$$\sigma_x^T = \frac{E_x T(z)}{1 - v_x v_y}(\alpha_x + \alpha_y v_y) \tag{15}$$

$$\sigma_y^T = \frac{E_y T(z)}{1 - v_x v_y}(\alpha_y + \alpha_x v_x) \tag{16}$$

$$\tau_{xy}^T = 0 \tag{17}$$

where α_x and α_y are the coefficients of thermal expansion in the x- and y-directions, respectively. $T(z) = \Delta T_b + [(\Delta T_t - \Delta T_b)/h]$ is the linear variation of temperature along the thickness when we consider a non-uniform heating load. ΔT_t and ΔT_b represent the temperature variation at the top and bottom sides of the plate, respectively. If a uniformly distributed temperature is considered, the variation of temperature at the bottom is equal to that at the top of the plate (i.e., $\Delta T_b = \Delta T_t = \Delta T$). The in-plane shear

force is set as zero as it is not affected by the variation of temperature for thin rectangular plates [61, 62]. Based on this, the in-plane forces and the moments resulted by the thermal effect can be derived using Eqs. (15) – (17) as follows

$$N_x^T = \frac{E_x(\alpha_x + \alpha_y v_y)}{1 - v_x v_y} \int_{-h/2}^{h/2} T(z) dz \tag{18}$$

$$N_y^T = \frac{E_y(\alpha_y + \alpha_x v_x)}{1 - v_x v_y} \int_{-h/2}^{h/2} T(z) dz \tag{19}$$

$$M_x^T = \frac{E_x(\alpha_x + \alpha_y v_y)}{1 - v_x v_y} \int_{-h/2}^{h/2} T(z) z dz \tag{20}$$

$$M_y^T = \frac{E_y(\alpha_y + \alpha_x v_x)}{1 - v_x v_y} \int_{-h/2}^{h/2} T(z) z dz \tag{21}$$

In this work, a uniformly distributed heating load is considered (i.e., $T(z) = \Delta T$). The positive value of ΔT results in a compressive force N^T. Eqs. (18) – (21) can be simplified as

$$N_x^T = \frac{E_x h \Delta T(\alpha_x + \alpha_y v_y)}{1 - v_x v_y} \tag{22}$$

$$N_y^T = \frac{E_y h \Delta T(\alpha_y + \alpha_x v_x)}{1 - v_x v_y} \tag{23}$$

$$M_x^T = M_y^T = 0 \tag{24}$$

For the isotropic case, the in-plane forces and the moments due to the thermal effect can be further simplified by setting $\alpha_x = \alpha_y = \alpha$ and taking the conditions in Eq. (2) for consideration. For generality and simplicity, the following dimensionless parameters are introduced for the case of orthotropic plates:

$$X = \frac{x}{L_1}, \quad Y = \frac{y}{L_2}, \quad W = \frac{w}{L_1}, \quad \lambda = \frac{L_1}{L_2}, \quad \Omega = \omega L_1^2 \sqrt{\frac{\rho h}{D_x}} \tag{25}$$

where ω is a circular frequency. Take a crack ($L_c = 2a$) along the x-axis as an example, and substitute the crack terms and the thermal terms into Eq. (1). Then, we have

$$\begin{aligned}
&\frac{\partial^4 W}{\partial X^4}+2\frac{B_o\lambda^2}{D_x}\frac{\partial^4 W}{\partial X^2 Y^2}+\lambda^4\frac{D_y}{D_x}\frac{\partial^4 W}{\partial Y^4}\\
&=\Omega^2 W-\frac{L_1^{\,2}}{D_x}\left[\frac{E_x h\Delta T(\alpha_x+\alpha_y v_y)}{1-v_x v_y}\frac{\partial^2 W}{\partial X^2}+\lambda^2\frac{E_y h\Delta T(\alpha_y+\alpha_x v_x)}{1-v_x v_y}\frac{\partial^2 W}{\partial Y^2}\right]\\
&+A\frac{D_y}{D_x}\left(\lambda^4\frac{\partial^4 W}{\partial Y^4}+v_x\lambda^2\frac{\partial^4 W}{\partial X^2 Y^2}\right)\\
&-B\frac{L_1^{\,2}}{D_x}\frac{E_y h\Delta T(\alpha_y+\alpha_x v_x)}{1-v_x v_y}\left(\lambda^2\frac{\partial^2 W}{\partial Y^2}\right)+\frac{L_1^{\,4}P_z}{D_x}
\end{aligned}\tag{26}$$

where

$$A=\frac{2a}{3\left(\alpha_{bt}^{o}/6+\alpha_{bb}^{o}\right)(3+v_x)(1-v_x)h+2a}\tag{27}$$

$$B=\frac{2a}{(6\alpha_{tb}^{o}+\alpha_{tt}^{o})(1-v_x^{\,2})h+2a}\tag{28}$$

For a free vibration analysis, we set $P_z=0$ in Eq. (26).

It is worth noting that the model expressed in Eq. (26) without the thermal effect can be degenerated to the models for isotropic plates and orthotropic plates proposed by Israr *et al.* [12] and Joshi *et al.* [22], respectively. If a crack ($L_c=2b$) along the *y*-axis is considered, the governing equations for the isotropic and orthotropic cracked plates can be derived in a similar way. To save space, these procedures are not repeated herein.

3. Thermal buckling analysis and critical temperature

Instability of engineering structures under thermal effects is a potential failure mode to induce thermal buckling. This is a phenomenon governed by the effects of in-plane thermal force and plate stiffness. Jones [61] provided a comprehensive study on the buckling analysis of plates. The study showed that the change of temperature with a uniform heating throughout the volume of a plate would cause buckling. In this section, a thin rectangular plate with bi-directionally restrained edges is considered to obtain the critical buckling temperature. An orthotropic rectangular plate with four simply supported edges is illustrated in Fig. 3. The material properties are assumed to

be independent of temperature. A uniformly distributed heating load is considered, thus the bending moments M^T_x and M^T_y are zero due to the uniform variation of temperature, and only the in-plane forces N^T_x and N^T_y are included. It is known that the natural frequency of an intact plate is zero at the critical buckling temperature [63]. This finding can also be applied to cracked plates. The equilibrium equation of orthotropic plates with a crack under the critical buckling temperature can be written as

$$\begin{aligned} &D_x \frac{\partial^4 w}{\partial x^4} + 2B_o \frac{\partial^4 w}{\partial x^2 y^2} + D_y \frac{\partial^4 w}{\partial y^4} \\ &= -\frac{E_x h T_{cr}(\alpha_x + \alpha_y v_y)}{1 - v_x v_y} \frac{\partial^2 w}{\partial x^2} - \frac{E_y h T_{cr}(\alpha_y + \alpha_x v_x)}{1 - v_x v_y} \frac{\partial^2 w}{\partial y^2} \\ &+ AD_y \left(\frac{\partial^4 w}{\partial y^4} + v_x \frac{\partial^4 w}{\partial x^2 y^2} \right) - B \frac{E_y h T_{cr}(\alpha_y + \alpha_x v_x)}{1 - v_x v_y} \frac{\partial^2 w}{\partial y^2} \end{aligned} \tag{29}$$

The general solution of Eq. (29) is assumed as

$$w(x, y) = W_{mn} \sin\left(\frac{m\pi}{L_1} x \right) \sin\left(\frac{n\pi}{L_2} y \right) \tag{30}$$

where m and n are the number of half sine waves in the x- and y-directions, respectively. The critical buckling temperature T_{cr} is given as

$$T_{cr} = \frac{h^2 \pi^2}{12 L_1^2} \left[\frac{D_x m^4 + 2B_o \lambda^2 m^2 n^2 + D_y \lambda^4 n^4 - AD_y (\lambda^4 n^4 + v_x \lambda^2 m^2 n^2)}{D_x (\alpha_x + \alpha_y v_y) m^2 + (1 + B) D_y (\alpha_y + \alpha_x v_x) \lambda^2 n^2} \right] \tag{31}$$

where $\lambda = L_1/L_2$ is the aspect ratio. While for the isotropic case, the critical buckling temperature becomes

$$T_{cr} = \frac{h^2 \pi^2}{12(1 + v)\alpha} \left[\frac{(m^2 + \lambda^2 n^2)^2 - A(\lambda^4 n^4 + v \lambda^2 m^2 n^2)}{L_1^2 (m^2 + \lambda^2 n^2 + B \lambda^2 n^2)} \right] \tag{32}$$

To investigate the crack effect on the thermal buckling of orthotropic plates with uniaxially in-plane restrained edges. Two cases of cracked orthotropic plates under a uniform heating load are presented and discussed. First, a uni-axially in-plane restrained orthotropic plate is considered, the fibers are along the x-direction (parallel to the in-plane restrained direction) as illustrated in Fig. 4(a). The boundaries of this orthotropic plate are treated as SS*SS*, where the S* boundary is still a simply

supported condition but it is able to produce deflections along the *y*-direction. In this case, a uniform heating load is applied on the plate, there are no any thermal forces and moments developed in the *y*-direction. Hence, the in-plane forces are expressed as

$$N_x^T = E_x \alpha_x h \Delta T \tag{33}$$

$$N_y^T = 0 \tag{34}$$

Similar to the situation of the crack plate with four simply supported edges in the presence of thermal loads, the governing equation can be derived from Eq. (1) by substituting Eqs. (33) – (34), we have

$$\begin{aligned} &D_x \frac{\partial^4 w}{\partial x^4} + 2B_o \frac{\partial^4 w}{\partial x^2 y^2} + D_y \frac{\partial^4 w}{\partial y^4} \\ &= -E_x h T_{cr} \alpha_x \frac{\partial^2 w}{\partial x^2} + AD_y \left(\frac{\partial^4 w}{\partial y^4} + v_x \frac{\partial^4 w}{\partial x^2 y^2} \right) \end{aligned} \tag{35}$$

The solution can be obtained by utilizing Eq. (30) and setting n = 1. Then, the critical buckling temperature is written as

$$T_{cr} = \frac{h^2 \pi^2}{12 L_1^{\,2} (1 - v_x v_y) \alpha_x} \left[m^2 + \frac{2B_o}{D_x} \lambda^2 + \frac{E_y \lambda^4}{E_x m^2} - \frac{A E_y (\lambda^4 + v_x m^2 \lambda^2)}{E_x m^2} \right] \tag{36}$$

In Fig. 4(b), we consider an orthotropic plate (S*SS*S) with in-plane restraints parallel to the *y*-direction. The in-plane forces are

$$N_x^T = 0 \tag{37}$$

$$N_y^T = E_y \alpha_y h \Delta T \tag{38}$$

Based on these conditions, the equation of motion becomes

$$\begin{aligned} &D_x \frac{\partial^4 w}{\partial x^4} + 2B_o \frac{\partial^4 w}{\partial x^2 y^2} + D_y \frac{\partial^4 w}{\partial y^4} \\ &= -E_y h T_{cr} \alpha_y (1 + B) \frac{\partial^2 w}{\partial y^2} + AD_y \left(\frac{\partial^4 w}{\partial y^4} + v_x \frac{\partial^4 w}{\partial x^2 y^2} \right) \end{aligned} \tag{39}$$

and the critical buckling temperature is

$$T_{cr} = \frac{h^2 \pi^2}{12 L_1^{\,2} (1 - v_x v_y)(1 + B) \alpha_y} \left[\frac{E_x}{E_y n^2 \lambda^2} + \frac{2B_o}{D_y} + n^2 \lambda^2 - A(n^2 \lambda^2 + v_x) \right] \tag{40}$$

From the equations of critical buckling temperature, it is noted that the critical values depend on the plate aspect ratio, elasticity constants, thermal expansion coefficients as well as plate thickness. The minimum value is obtained by setting $m = 1$ and $n = 1$ to satisfy the material properties mentioned above and by keeping good consistence for comparison. The thermal buckling temperature can be reduced to the expression proposed by Jones [64] for orthotropic plates without a surface crack.

4. Solution methodology

In this section, the DSC algorithm is briefly introduced. To approximate the derivative of a function with respect to a spatial variable at a given discrete point, a weighted linear combination of the function values at the uniformly distributed points ($2M+1$) is employed, where M is known as a half bandwidth. The n^{th} derivative of a function $f(x)$ at the i^{th} point is approximated as [38]

$$f^{(n)}(x_i) = \sum_{j=-M}^{M} C_{i,j}^{n} f(x_{i+j}), \qquad i = 0,1,...,N-1 \tag{41}$$

where $C_{i,j}$ are the weighting coefficients calculated by the DSC kernel. $f(x_{i+j})$ is regarded as a trial function in this discrete form. $\delta_{\alpha,\Delta}$ is a delta kernel of the Dirichlet type and its n^{th} derivatives with respect to x is given by

$$\delta_{\alpha,\Delta}^{(n)}(x - x_k) = \left(\frac{d}{dx}\right)^{n} \delta_{\alpha,\Delta}^{(n)}(x - x_k) \tag{42}$$

where Δ is a grid spacing. Therefore, the n^{th}-order derivatives of the function $f(x)$ with respect to x can be discretized as

$$f^{(n)}(x_i) = \sum_{k=-M}^{M} \delta_{\alpha,\Delta}^{(n)} f(x_k) \tag{43}$$

It is worth noting that some computational methods, including Galerkin approach and finite difference method, can be derived from a single starting point by the implementation of the DSC method to offer a unified representation [39]. Based on Eq. (43), a small matrix-band can be formulated for the approximation of partial derivatives

in terms of the DSC approach. This enhances the computational efficiency in dealing with large-scale structural calculations. In addition, the controllable matrix bandwidth is able to optimize the accuracy and convergence for practical applications [39, 65]. In addition, the numerical stability of the DSC method over other numerical methods (e.g., differential quadrature method) has also been authenticated in high-frequency analysis of plates [36, 38, 57]. According to the DSC algorithm, the weighting coefficients for the calculation of derivatives at each point involve relevant fictitious/ghost points outside the physical domain of rectangular plates. The elimination of fictitious/ghost points corresponding to general boundary conditions, namely simply supported, clamped and free edges, is discussed in the subsequent sections.

4.1. Formulation of DSC approach

In this work, the regularized Shannon's delta kernel (RSK) [34, 35] is considered as

$$\delta_{\alpha,\Delta}^{(n)}(x-x_k)=\frac{\sin[(\pi/\Delta)(x-x_k)]}{(\pi/\Delta)(x-x_k)}\exp\left[-\frac{(x-x_k)^2}{2\sigma^2}\right] \tag{44}$$

where σ is a controllable parameter to determine the effective computational bandwidth [66]. To conduct the dynamic analysis of a rectangular plate by the DSC method, a uniform distribution of grid points on the domain of a rectangular plate is considered. In Fig. 5, we consider a uniform grid with 7 points ($N = 7$) in the plate as an example for illustration. Then, we have

$$0=X_0<X_1<...<X_{N_X}=1, \tag{45}$$

and

$$0=Y_0<Y_1<...<Y_{N_Y}=1. \tag{46}$$

To formulate an eigenvalue problem in terms of the DSC approach, a column vector **W** is introduced as [40]

$$\mathbf{W}=(W_{0,0},...,W_{0,N_Y},W_{1,0},...,W_{N_X,N_Y})^{\mathrm{T}} \tag{47}$$

where $W_{i,j} = W(X_i, Y_i)(i = 0, 1, \ldots, N_X ; i = 0, 1, \ldots, N_Y)$ denotes the transverse displacement of an arbitrary grid point in a rectangular plate. Then, we define the $(N_q+1) \times (N_q+1)$ differential matrix $\mathbf{D}_q^n (q = X, Y; n = 1, 2, \ldots)$, with the elements given by

$$[\mathbf{D}_q^n]_{i,j} = \delta_{\alpha,\Delta}^{(n)}(q_i - q_j), \qquad i, j = 0,1,...,N_q \tag{48}$$

where

$$\delta_{\alpha,\Delta}^{(n)}(q_i - q_j) = \left[\left(\frac{d}{dq}\right)^n \delta_{\alpha,\Delta}^{(n)}(q - q_j)\right]_{q=q_i} = C_m^n \tag{49}$$

in which $m = (q_i - q_j)/\Delta$. The matrix $\mathbf{D}$ is banded to $i-j = m = -M, \ldots, 0, \ldots, M$. Eventually, the governing equation in Eq. (26) for the free vibration of cracked orthotropic rectangular plates under a thermal load can be expressed as

$$\begin{aligned}
&\left(\mathbf{D}_X^4 \otimes \mathbf{I}_Y + 2\frac{B_o\lambda^2}{D_x}\mathbf{D}_X^2 \otimes \mathbf{D}_Y^2 + \lambda^4\frac{D_y}{D_x}\mathbf{I}_X \otimes \mathbf{D}_Y^4\right)\mathbf{W} \\
&= \Omega^2\mathbf{W} - \frac{L_1^2}{D_x}\left[\frac{E_x h\Delta T(\alpha_x + \alpha_y v_y)}{1 - v_x v_y}\mathbf{D}_X^2 \otimes \mathbf{I}_Y + \lambda^2\frac{E_y h\Delta T(\alpha_y + \alpha_x v_x)}{1 - v_x v_y}\mathbf{I}_X \otimes \mathbf{D}_Y^2\right]\mathbf{W} \\
&+ A\frac{D_y}{D_x}(\lambda^4\mathbf{I}_X \otimes \mathbf{D}_Y^4 + v_x\lambda^2\mathbf{D}_X^2 \otimes \mathbf{D}_Y^2)\mathbf{W} \\
&- B\frac{L_1^2}{D_x}\frac{E_y h\Delta T(\alpha_y + \alpha_x v_x)}{1 - v_x v_y}(\lambda^2\mathbf{I}_X \otimes \mathbf{D}_Y^2)\mathbf{W}
\end{aligned} \tag{50}$$

where $\mathbf{I}_q$ is the $(N_q+1) \times (N_q+1)$ unit matrix and $\otimes$ denotes the tensional product. The governing equation for the isotropic case can be obtained using Eq. (2) together with the condition $\alpha_x = \alpha_y = \alpha$ in a similar way.

4.2. Elimination of fictitious/ghost points

The basic rationale for elimination of fictitious/ghost points generated from the calculation procedures is to establish the relationship between the inner points and the outer points of the physical domain of rectangular plates. The imposition of boundary constraints is different for the following three classical boundaries:

- Simply supported edge (S):

$$w_x = M_x = 0, \qquad w_y = M_y = 0. \tag{51}$$

- Clamped edge (C):

$$w_x = \frac{\partial w}{\partial x} = 0, \qquad w_y = \frac{\partial w}{\partial y} = 0. \tag{52}$$

- Free edge (F):

$$Q_x = M_x = 0, \qquad Q_y = M_y = 0 \quad \text{and} \quad R = 0. \tag{53}$$

where w_i ($i = x, y$) are the transverse displacements, M_i ($i = x, y$) are the bending moments, Q_i ($i = x, y$) are the shear forces and R is the corner force. The expressions for the corner force, bending moments and shear forces are presented in Appendix A.

For the treatment of simply supported and clamped boundaries, the anti-symmetric and symmetric extension methods can be, respectively, applied to the elimination of fictitious points [65-67]. Take the left edge of a rectangular plate as an example (see Fig. 5), the relationship between the inner nodes and the outer nodes is assumed as

$$W(X_{-m}) - W(X_0) = a_m[W(X_m) - W(X_0)] \tag{54}$$

which can be written as

$$W(X_{-m}) = a_m W(X_m) + (1 - a_m) W(X_0) \tag{55}$$

The first and second-order derivatives of W can be approximated as

$$\begin{aligned} W'(X) &= \sum_{m=-M}^{M} C_m^1 W(X_m) \\ &= \left[C_0^1 - \sum_{m=1}^{M} (1 - a_m) C_m^1 \right] W(X_0) + \sum_{m=1}^{M} (1 - a_m) C_m^1 W(X_m) \end{aligned} \tag{56}$$

$$\begin{aligned} W''(X) &= \sum_{m=-M}^{M} C_m^2 W(X_m) \\ &= \left[C_0^2 + \sum_{m=1}^{M} (1 - a_m) C_m^2 \right] W(X_0) + \sum_{m=1}^{M} (1 + a_m) C_m^2 W(X_m) \end{aligned} \tag{57}$$

In a similar way, higher-order derivatives can be obtained. By employing the boundary conditions given in Eqs. (51) and (52), one obtains $a_m = -1$ for a simply

supported edge and $a_m = 1$ for a clamped edge. The governing equations of the isotropic and orthotropic rectangular plates, expressed in the following matrix form, can be solved by using a standard eigenvalue solver.

$$[\mathbf{K}]\mathbf{W} = \Omega^2\mathbf{W} \tag{58}$$

However, it is limited for the treatment of free boundary conditions using the anti-symmetric and symmetric extension methods. In the literature [68, 69], the iteratively matched boundary and the matched interface and boundary method were proposed to address the vibration problem of plates and beams with free edges. Recently, a new scheme that incorporates the DSC method with the Taylor series expansion method has been proposed for the analysis of rectangular plates with free edges [58]. Making use of a Taylor series, a function $f(x)$ at $x = 0$ can be defined as

$$f(x) = f(0) + f'(0)x + \frac{f''(0)x^2}{2!} + \frac{f'''(0)x^3}{3!} + \frac{f^{IV}(0)x^4}{4!} + \frac{f^{V}(0)x^5}{5!}... \tag{59}$$

The sum of $W(X)$ and $W(-X)$ expanded in terms of a Taylor series at $X = 0$ can be written as

$$W(-X) = -W(X) + 2W(X_0) + W''(X_0)X^2 + \frac{1}{12}W^{IV}(X_0)X^4..., \quad X > 0 \tag{60}$$

where the derivative terms $W''(X_0)$ and $W^{IV}(X_0)$ are the additional degree of freedoms. It is noted that the maximum degree of freedoms must be less than or equal to the sum of the governing equations together with the number of boundary conditions. To eliminate the fictitious/ghost points, Eq. (60) is reduced to

$$W(-X) = -W(X) + 2W(X_0) + W''(X_0)X^2 + \frac{1}{12}W^{IV}(X_0)X^4, \quad X > 0 \tag{61}$$

and

$$W(-X) = -W(X) + 2W(X_0) + W''(X_0)X^2, \quad X > 0 \tag{62}$$

The governing equation of a rectangular plate with free edges is a fourth-order differential equation. Eq. (61) is used to calculate the weighting coefficients of the third- and fourth-order derivatives, while Eq. (62) is applied to obtain the weighting coefficients of the first- and second-order derivatives to prevent the generation of

higher-order mixed products of these additional degree-of-freedoms. After eliminating the fictitious/ghost points at both sides of the plate by using Eqs. (61) and (62), we derive

$$W'(X)=\sum_{m=0}^{N_X} C_m^1 W(X_m) + C_{N_X+1}^1 W''(X_0)+(0)\cdot W^{IV}(X_0)+C_{N_X+3}^1 W''(X_{N_X})+(0)\cdot W^{IV}(X_{N_X}) \tag{63}$$

$$W''(X)=\sum_{m=0}^{N_X} C_m^2 W(X_m) + C_{N_X+1}^2 W''(X_0)+(0)\cdot W^{IV}(X_0)+C_{N_X+3}^2 W''(X_{N_X})+(0)\cdot W^{IV}(X_{N_X}) \tag{64}$$

$$W'''(X)=\sum_{m=0}^{N_X} C_m^3 W(X_m) + C_{N_X+1}^3 W''(X_0)+C_{N_X+2}^3 W^{IV}(X_0)+C_{N_X+3}^3 W''(X_{N_X})+C_{N_X+4}^3 W^{IV}(X_{N_X}) \tag{65}$$

$$W^{IV}(X)=\sum_{m=0}^{N_X} C_m^1 W(X_m) + C_{N_X+1}^4 W''(X_0)+C_{N_X+2}^4 W^{IV}(X_0)+C_{N_X+3}^4 W''(X_{N_X})+C_{N_X+4}^4 W^{IV}(X_{N_X}) \tag{66}$$

The additional derivatives of the boundary points are assumed to be set at two sides of the rectangular plate as shown in Fig. 5. These degree-of-freedoms are assigned as $W''(0)$, $W^{IV}(0)$, $W''(N-1)$ and $W^{IV}(N-1)$ in respect to the *x*- and *y*-directions and their products correspond to the corner points. According to Eqs. (63) – (66), only four products (i.e., $p1$, $p2$, $p3$ and $p4$ in Fig. 5) of $W''(X_0)$, $W''(Y_0)$, $W''(X_{N_X})$ and $W''(Y_{N_Y})$ will be generated by the mixed-order derivatives of the governing equation. The total number of degree-of-freedoms is equal to N^2+8N+4 as illustrated in Fig. 5. Using the governing equations for every inner and edge points, we put $M=0$ and $Q=0$ in the boundary conditions of Eq. (53) on the outer nodes located at the green dash line and the red dash line, respectively. The equations related to the corner force $R=0$ are placed at $p1$ – $p4$. By properly rearranging the displacement vectors, the eigenvalue problem can be expressed in a partitioned matrix form as

$$\begin{bmatrix} \mathbf{K}_{\mathbf{II}} & \mathbf{K}_{\mathbf{IA}} \\ \mathbf{K}_{\mathbf{AI}} & \mathbf{K}_{\mathbf{AA}} \end{bmatrix} \begin{Bmatrix} \mathbf{W}_{\mathbf{I}} \\ \mathbf{W}_{\mathbf{A}} \end{Bmatrix} = \Omega^2 \begin{bmatrix} \mathbf{I} & \mathbf{0} \\ \mathbf{0} & \mathbf{0} \end{bmatrix} \begin{Bmatrix} \mathbf{W}_{\mathbf{I}} \\ \mathbf{W}_{\mathbf{A}} \end{Bmatrix} \tag{67}$$

where $\mathbf{W_I}$ and $\mathbf{W_A}$ denote the transverse displacements of the inner points and the additional points, respectively. Eq. (67) can be further simplified by eliminating the vector $\mathbf{W_A}$ to form a final global one as

$$[\bar{\mathbf{K}}]\mathbf{W}_{\mathbf{I}} = \Omega^2 \mathbf{W}_{\mathbf{I}} \tag{68}$$

5. Results and Discussion

This section presents the results for the free vibration analysis of isotropic and orthotropic rectangular plates with three types of boundary conditions stated in Eqs. (51) – (53). The effects of the surface part-through crack and the thermal load on the dynamic behavior of isotropic and orthotropic rectangular plates are discussed. The natural frequencies are expressed in terms of a non-dimensional form as $\Omega = \omega L_1^2 \sqrt{\rho h / D}$. In all computational cases, the number of grid points and the half bandwidth used are N = 32 and M = 25, respectively. To show the effect of the half bandwidth M, a simple convergence study for CCCC square plates is presented in Fig. 6 for illustration.

The free vibration of intact isotropic plates (i.e., SSSS, CCCC and FFFF) is analyzed by the DSC method and the first five mode frequencies are presented in Tables 1 – 3, respectively. The material properties of the isotropic plates are taken as Young's modulus E = 207 GPa, Poisson's ratio v = 0.3 and density ρ = 7850 kg/m^3. Two aspect ratios (λ = 1 and λ = 1.5) are presented for the vibration analysis of SSSS and CCCC plates for validation. The results obtained by the DSC method in Tables 1 – 3 show good agreement with the published results [70]. It is found that the results for the fully clamped isotropic plate are consistently smaller than those results obtained by Leissa [70]. In Fig. 6, the convergence study is to confirm the correctness and reliability of the results. In Table 2, the present results are also compared with those from other

numerical methods, including the mixed finite element-Ritz method and the differential quadrature method [38, 71, 72]. This comparison also indicates that the DSC method is consistent with other numerical approaches and can achieve a high confidence level. The use of the Taylor series expansion method is applied to address the rectangular plates with free edges. In Table 3, the first five vibration mode frequencies presented by the DSC method are compared with the results given by Leissa and Narita [73], Gorman [74] and Wang *et al.* [75], all of them are in good agreement.

To investigate the crack effect, the LSM-based analytical model provided by the works in [12, 14] are utilized. The crack is a continuous surface part-through crack that is located at the center of the plates. The parameter value ($\zeta = d/h$) is assumed to 0.6. Four boundary cases, SSSS, CCCC, SSFF and SCFF, with different crack length ratios ($2a/L_1 = 0 - 0.2$) are considered for free vibration analysis. The first three vibration frequencies are summarized in Table 4 and Table 5. We observe that the natural frequency decreases as the crack length increases. The present results of SSSS plate and CCCC plate are very close to those of Soni *et al.* [76]. In the open literature, the solutions for cracked thin plates with free edges are unavailable. Hence, SSFF and SCFF plates with different degrees of damage are analyzed and the results are presented in Table 5, in which the first mode natural frequency is compared with the accurate results from Leissa [70].

In Fig. 7, the first four mode shapes of a simply supported plate are depicted. In this case, the aspect ratio of the plate is taken as 1, and the crack length ratios are 0 and 0.2. In the contour plots, the second to fourth mode shapes are switched when there is a surface crack on the plate. Fig. 8 presents the effect of a crack on the vibration mode shapes of the clamped plate. The results are similar to those results of the SSSS case. It is concluded that a surface crack can change the dynamic behavior of rectangular plates. The present results of the orthotropic plates with different combinations of boundaries are compared with those obtained by the differential quadrature method [77] in Table 6, wherein the material properties are set as $E_x/E_y = 2.45$, $\nu_x = 0.23$ and $G_{xy}/E_y = 0.48$. The

results indicate that the DSC method achieves a high level of accuracy for various boundary conditions. The variation of natural frequencies of the orthotropic plates (i.e., SFFF and SCFF cases) due to the crack effect can be observed in Fig. 9. The reduction of the fundamental frequency is observed as the crack length increases.

To investigate the thermal effect on the dynamic responses of rectangular plates with or without crack, the isotropic and orthotropic material properties are listed in Table 7 and Table 8, respectively. The analytical model of cracked thin plates in thermal environment is based on the classical plate theory and the crack is formulated by the LSM. The value of $\zeta = d/h$ in the LSM is assumed to 0.6. The critical buckling temperature of cracked rectangular plates can be calculated using Eq. (31) and Eq. (32), see Table 9. A validation of the critical buckling temperature of cracked plates is carried out by comparing the results from the literature. The change of the critical buckling temperature with a surface crack for the isotropic and orthotropic square plates is presented in Figs. 10 and 11. It is seen that the critical buckling temperature for both types of plates would decrease as the crack length increases. Because of the enforced fibers, the orthotropic plate holds a higher critical buckling temperature than the isotropic one.

The uniform rise in temperature is expressed as a non-dimensional variation of temperature $T^* = \Delta T/T_{cr}$, where ΔT is the rise in temperature. Table 10 presents the fundamental frequency of SSSS orthotropic plates for various crack length ratios under the thermal condition of $T^* = 0$. The results of the DSC method are very close to the existing results from the Galerkin method [33]. In Tables 11 and 12, the rise of temperature can affect the fundamental frequency of the isotropic and orthotropic plates with or without cracks. We observe that a higher variation of temperature occurs, it will reduce the natural frequency of the isotropic and orthotropic plates.

In addition, the crack effect on the thermal buckling of uni-axially restrained orthotropic plates is also investigated. A special restrained manner of the simply supported condition is defined and marked as S*. This edge condition is permissible for

in-plane movement as shown in Fig. 4. The variation of the fundamental frequency with a uniform rise of temperature from 0 to $0.9T_{cr}$ for SS*SS* and S*SS*S orthotropic plates with or without crack is presented in Fig. 12. It is seen that, for both plates, the presence of the thermal effect would decrease the fundamental frequency and the crack effect would reduce the critical buckling temperature. Fig. 11 shows the variation of critical buckling temperature for square plates (SS*SS* and S*SS*S) subject to various crack length ratios and different directions. It is observed that the S*SS*S orthotropic plate has a higher critical buckling temperature than the SS*SS* orthotropic plate. This is due to the directional nature of rigidity and the coefficient of thermal expansion. For the S*SS*S plate, a uniform heating load is able to cause the displacement parallel to the *x*-axis, it is subject to a lower coefficient of thermal expansion along this direction. In short, the permissible direction of in-plane movements along the fibers can cause a higher critical buckling temperature. In Figs. 10 – 11, it is also found that the influence of the crack effect along the fibers is less than the crack effect across the fibers on the critical buckling temperature. This is consistent with the conclusion presented by Joshi *et al.* [33].

6. Conclusions

This research work presents the free vibration and buckling analysis of thin rectangular isotropic and orthotropic plates in thermal environment. Both intact and cracked plates are subject to uniform temperature heating loads. The surface crack on the plates is considered as a continuous part-through surface line that is formulated by the line-spring model. Based on the mathematical models, the DSC method is first applied to address the free vibration problem of cracked isotropic and orthotropic plates in the presence of thermal environment. By incorporating with the Taylor series expansion technique, the DSC method is not restricted to the plate problems with free boundary conditions. The influence of crack length, aspect ratio, boundary condition and thermal load on the dynamic responses of the isotropic plates and orthotropic plates

is considered herein. Based on the results, one may conclude that the presented scheme can achieve a high level of reliability and accuracy. Its computational efficiency due to the small-band-matrix approximation leads to a potential use in dealing with large-scale structural calculations. On the other hand, it is found that the presence of cracks not only affects the natural frequencies, but also switches its corresponding mode shapes as well as critical buckling temperature. As the temperature rises and the crack length increases, the vibration frequency of the plates would decrease. This is mainly due to the change of material properties under these effects. In the buckling analysis, the results imply that the critical buckling temperature would be reduced as the crack length increases. In addition, the variation of critical buckling temperature is more pronounced in the case of a crack across the fibers. To compare with the published results, the present solutions can provide excellent agreement. Based on its accuracy, accurate first-known solutions are also presented.

In reality, the presence of cracks or defects in the structural elements is much more stochastic and complicated. This research is first put forward to employ the DSC method in free vibration analysis and buckling analysis of cracked plates. In the future work, the possibility of its potential applications will also be explored in structural health monitoring.

Acknowledgements

The work described in this paper was supported by the Early Career Scheme from the Research Grants Council of the Hong Kong Special Administrative Region (Project No. PolyU 252026/16E) and the National Natural Science Foundation of China (Grant No. 11602210). We also thank the anonymous reviewers for their constructive comments.

References

[1] A. W. Leissa, *Vibration of plates*. Scientific and Technical Information Office, National Aeronautics and Space Administration Washington, 1969.

[2] A. W. Leissa, *Vibration of shells*. Scientific and Technical Information Office, National Aeronautics and Space Administration Washington, 1973.

[3] S. P. Timoshenko, *Theory of Elastic Stability, by S. Timoshenko*. McGraw-Hill Book Company, Incorporated, 1936.

[4] S. P. Timoshenko and S. Woinowsky-Krieger, *Theory of plates and shells*. McGraw-hill, 1959.

[5] C. Wang, Y. Xiang, S. Kitipornchai, and K. Liew, "Buckling solutions for Mindlin plates of various shapes," *Engineering Structures,* vol. 16, no. 2, pp. 119-127, 1994.

[6] C. Feng, S. Kitipornchai, and J. Yang, "Nonlinear free vibration of functionally graded polymer composite beams reinforced with graphene nanoplatelets (GPLs)," *Engineering Structures,* vol. 140, pp. 110-119, 2017.

[7] J. R. Rice and N. Levy, "The part-through surface crack in an elastic plate," *Journal of Applied Mechanics,* vol. 39, no. 1, pp. 185-194, 1972.

[8] G. R. Irwin, "Crack-extension force for a part-through crack in a plate," *Journal of Applied Mechanics,* vol. 29, no. 4, pp. 651-654, 1962.

[9] S. E. Khadem and M. Rezaee, "An analytical approach for obtaining the location and depth of an all-over part-through crack on externally in-plane loaded rectangular plate using vibration analysis," *Journal of Sound and Vibration,* vol. 230, no. 2, pp. 291-308, 2000.

[10] C. Huang, A. Leissa, and C. Chan, "Vibrations of rectangular plates with internal cracks or slits," *International Journal of Mechanical Sciences,* vol. 53, no. 6, pp. 436-445, 2011.

[11] S. Hosseini-Hashemi, H. R. Gh, and H. R. DT, "Exact free vibration study of rectangular Mindlin plates with all-over part-through open cracks," *Computers & Structures,* vol. 88, no. 17-18, pp. 1015-1032, 2010.

[12] A. Israr, M. P. Cartmell, E. Manoach, I. Trendafilova, M. Krawczuk, and Ĺ. Arkadiusz, "Analytical modeling and vibration analysis of partially cracked rectangular plates with different boundary conditions and loading," *Journal of Applied Mechanics,* vol. 76, no. 1, p. 011005, 2009.

[13] B. Aksel and F. Erdogan, "Interaction of part-through cracks in a flat plate," 1985.

[14] P. Joshi, N. Jain, and G. Ramtekkar, "Analytical modeling and vibration analysis of internally cracked rectangular plates," *Journal of Sound and Vibration,* vol. 333, no. 22, pp. 5851-5864, 2014.

[15] T. Bose and A. Mohanty, "Vibration analysis of a rectangular thin isotropic plate with a part-through surface crack of arbitrary orientation and position," *Journal of Sound and Vibration,* vol. 332, no. 26, pp. 7123-7141, 2013.

[16] K. Liew, K. Hung, and M. Lim, "A solution method for analysis of cracked plates under vibration," *Engineering Fracture Mechanics,* vol. 48, no. 3, pp. 393-404, 1994.

[17] C. Huang and A. Leissa, "Vibration analysis of rectangular plates with side cracks via the Ritz method," *Journal of Sound and Vibration,* vol. 323, no. 3-5, pp. 974-988, 2009.

[18] Z. Xu and W. Chen, "Vibration Analysis of Plate with Irregular Cracks by Differential Quadrature Finite Element Method," *Shock and Vibration,* vol. 2017, 2017.

[19] Y. Xing and B. Liu, "New exact solutions for free vibrations of thin orthotropic rectangular plates," *Composite Structures,* vol. 89, no. 4, pp. 567-574, 2009.

[20] M. Biancolini, C. Brutti, and L. Reccia, "Approximate solution for free vibrations of thin orthotropic rectangular plates," *Journal of Sound and Vibration,* vol. 288, no. 1-2, pp. 321-344, 2005.

[21] L. Kurpa, V. Rvachev, and E. Ventsel, "The R-function method for the free vibration analysis of thin orthotropic plates of arbitrary shape," *Journal of Sound and Vibration,* vol. 261, no. 1, pp. 109-122, 2003.

[22] P. Joshi, N. Jain, and G. Ramtekkar, "Analytical modelling for vibration analysis of partially cracked orthotropic rectangular plates," *European Journal of Mechanics-A/Solids,* vol. 50, pp. 100-111, 2015.

[23] Y. Yum and C. Hong, "Stress intensity factors in finite orthotropic plates with a crack under mixed mode deformation," *International Journal of Fracture,* vol. 47, no. 1, pp. 53-67, 1991.

[24] A. Szekrényes, "Analysis of classical and first-order shear deformable cracked orthotropic plates," *Journal of Composite Materials,* vol. 48, no. 12, pp. 1441-1457, 2014.

[25] H.-S. Shen, Y. Chen, and J. Yang, "Bending and vibration characteristics of a strengthened plate under various boundary conditions," *Engineering Structures,* vol. 25, no. 9, pp. 1157-1168, 2003.

[26] N. Jadeja and T.-C. Loo, "Heat induced vibration of a rectangular plate," *Journal of Engineering for Industry,* vol. 96, no. 3, pp. 1015-1021, 1974.

[27] H.-S. Shen, "Thermal postbuckling behavior of imperfect shear deformable laminated plates with temperature-dependent properties," *Computer Methods in Applied Mechanics and Engineering,* vol. 190, no. 40-41, pp. 5377-5390, 2001.

[28] K. Zhou, J. Su, and H. Hua, "Closed Form Solutions for Vibration and Sound Radiation of Orthotropic Plates under Thermal Environment," *International Journal of Structural Stability and Dynamics,* p. 1850098, 2018.

[29] O. S. Sahin, A. Avci, and S. Kaya, "Thermal buckling of orthotropic plates with angle crack," *Journal of Reinforced Plastics and Composites,* vol. 23, no. 16, pp. 1707-1716, 2004.

[30] S. Natarajan, P. Baiz, M. Ganapathi, P. Kerfriden, and S. Bordas, "Linear free flexural vibration of cracked functionally graded plates in thermal

environment," *Computers & Structures,* vol. 89, no. 15-16, pp. 1535-1546, 2011.

[31] A. A. Rahimabadi, S. Natarajan, and S. P. Bordas, "Vibration of functionally graded material plates with cutouts & cracks in thermal environment," in *Key Engineering Materials*, 2013, vol. 560, pp. 157-180: Trans Tech Publ.

[32] P. Joshi, N. Jain, and G. Ramtekkar, "Effect of thermal environment on free vibration of cracked rectangular plate: An analytical approach," *Thin-Walled Structures,* vol. 91, pp. 38-49, 2015.

[33] P. Joshi, N. Jain, G. Ramtekkar, and G. S. Virdi, "Vibration and buckling analysis of partially cracked thin orthotropic rectangular plates in thermal environment," *Thin-Walled Structures,* vol. 109, pp. 143-158, 2016.

[34] G. Wei, "Discrete singular convolution for the solution of the Fokker–Planck equation," *The Journal of Chemical Physics,* vol. 110, no. 18, pp. 8930-8942, 1999.

[35] G. Wei, "A unified approach for the solution of the Fokker-Planck equation," *Journal of Physics A: Mathematical and General,* vol. 33, no. 27, p. 4935, 2000.

[36] Y. Zhao, G. Wei, and Y. Xiang, "Discrete singular convolution for the prediction of high frequency vibration of plates," *International Journal of Solids and Structures,* vol. 39, no. 1, pp. 65-88, 2002.

[37] G. Wei, Y. Zhao, and Y. Xiang, "A novel approach for the analysis of high-frequency vibrations," *Journal of Sound and Vibration,* vol. 257, no. 2, pp. 207-246, 2002.

[38] C. Ng, Y. Zhao, and G. Wei, "Comparison of discrete singular convolution and generalized differential quadrature for the vibration analysis of rectangular plates," *Computer Methods in Applied Mechanics and Engineering,* vol. 193, no. 23-26, pp. 2483-2506, 2004.

[39] G. W. Wei, Y. B. Zhao, and Y. Xiang, "Discrete singular convolution and its application to the analysis of plates with internal supports. Part 1: Theory and algorithm," *International Journal for Numerical Methods in Engineering,* vol. 55, no. 8, pp. 913-946, 2002.

[40] S. K. Lai and Y. Xiang, "DSC analysis for buckling and vibration of rectangular plates with elastically restrained edges and linearly varying in-plane loading," *International Journal of Structural Stability and Dynamics,* vol. 9, no. 03, pp. 511-531, 2009.

[41] S. K. Lai and Y. Xiang, "Buckling and vibration of elastically restrained standing vertical plates," *Journal of Vibration and Acoustics,* vol. 134, no. 1, p. 014502, 2012.

[42] Y. Hou, G. Wei, and Y. Xiang, "DSC-Ritz method for the free vibration analysis of Mindlin plates," *International Journal for Numerical Methods in Engineering,* vol. 62, no. 2, pp. 262-288, 2005.

[43] C. Lim, Z. Li, and G. Wei, "DSC-Ritz method for high-mode frequency analysis of thick shallow shells," *International Journal for Numerical Methods in Engineering,* vol. 62, no. 2, pp. 205-232, 2005.

[44] C. Lim, Z. Li, Y. Xiang, G. Wei, and C. Wang, "On the missing modes when using the exact frequency relationship between Kirchhoff and Mindlin plates," *Advances in Vibration Engineering,* vol. 4, no. 3, pp. 221-248, 2005.

[45] Ö. Civalek, "An efficient method for free vibration analysis of rotating truncated conical shells," *International Journal of Pressure Vessels and Piping,* vol. 83, no. 1, pp. 1-12, 2006.

[46] Ö. Civalek, "A parametric study of the free vibration analysis of rotating laminated cylindrical shells using the method of discrete singular convolution," *Thin-Walled Structures,* vol. 45, no. 7-8, pp. 692-698, 2007.

[47] Ö. Civalek, "Free vibration and buckling analyses of composite plates with straight-sided quadrilateral domain based on DSC approach," *Finite Elements in Analysis and Design,* vol. 43, no. 13, pp. 1013-1022, 2007.

[48] Ö. Civalek, "Free vibration of carbon nanotubes reinforced (CNTR) and functionally graded shells and plates based on FSDT via discrete singular convolution method," *Composites Part B: Engineering,* vol. 111, pp. 45-59, 2017.

[49] Q. Zhu and X. Wang, "Free vibration analysis of thin isotropic and anisotropic rectangular plates by the discrete singular convolution algorithm," *International Journal for Numerical Methods in Engineering,* vol. 86, no. 6, pp. 782-800, 2011.

[50] G. Duan and X. Wang, "Free vibration analysis of multiple-stepped beams by the discrete singular convolution," *Applied Mathematics and Computation,* vol. 219, no. 24, pp. 11096-11109, 2013.

[51] X. Wang and G. Duan, "Discrete singular convolution element method for static, buckling and free vibration analysis of beam structures," *Applied Mathematics and Computation,* vol. 234, pp. 36-51, 2014.

[52] G. Duan, X. Wang, and C. Jin, "Free vibration analysis of circular thin plates with stepped thickness by the DSC element method," *Thin-Walled Structures,* vol. 85, pp. 25-33, 2014.

[53] G. Duan and X. Wang, "Vibration analysis of stepped rectangular plates by the discrete singular convolution algorithm," *International Journal of Mechanical Sciences,* vol. 82, pp. 100-109, 2014.

[54] X. Wang, C. Xu, and S. Xu, "The discrete singular convolution for analyses of elastic wave propagations in one-dimensional structures," *Applied Mathematical Modelling,* vol. 34, no. 11, pp. 3493-3508, 2010.

[55] Y. Xiang, S. K. Lai, and L. Zhou, "DSC-element method for free vibration analysis of rectangular Mindlin plates," *International Journal of Mechanical Sciences,* vol. 52, no. 4, pp. 548-560, 2010.

[56] S. K. Lai, L. Zhou, Y. Zhang, and Y. Xiang, "Application of the DSC-Element method to flexural vibration of skew plates with continuous and discontinuous boundaries," *Thin-Walled Structures,* vol. 49, no. 9, pp. 1080-1090, 2011.

[57] X. Wang and S. Xu, "Free vibration analysis of beams and rectangular plates with free edges by the discrete singular convolution," *Journal of Sound and Vibration,* vol. 329, no. 10, pp. 1780-1792, 2010.

[58] X. Wang and Z. Yuan, "Discrete singular convolution and Taylor series expansion method for free vibration analysis of beams and rectangular plates with free boundaries," *International Journal of Mechanical Sciences,* vol. 122, pp. 184-191, 2017.

[59] S. E. Khadem and M. Rezaee, "Introduction of modified comparison functions for vibration analysis of a rectangular cracked plate," *Journal of Sound and Vibration,* vol. 236, no. 2, pp. 245-258, 2000.

[60] H. Okamura, H. Liu, C.-S. Chu, and H. Liebowitz, "A cracked column under compression," *Engineering Fracture Mechanics,* vol. 1, no. 3, pp. 547-564, 1969.

[61] R. M. Jones, *Buckling of bars, plates, and shells*. Bull Ridge Corporation, 2006.

[62] V. Birman, *Plate structures*. Springer Science & Business Media, 2011.

[63] K. Murphy, L. Virgin, and S. Rizzi, "The effect of thermal prestress on the free vibration characteristics of clamped rectangular plates: theory and experiment," *Journal of Vibration and Acoustics,* vol. 119, no. 2, pp. 243-249, 1997.

[64] R. M. Jones, "Thermal buckling of uniformly heated unidirectional and symmetric cross-ply laminated fiber-reinforced composite uniaxial in-plane restrained simply supported rectangular plates," *Composites Part A: Applied science and manufacturing,* vol. 36, no. 10, pp. 1355-1367, 2005.

[65] Y. Xiang, Y. B. Zhao, and G. W. Wei, "Discrete singular convolution and its application to the analysis of plates with internal supports. Part 2: Applications," *International Journal for Numerical Methods in Engineering,* vol. 55, no. 8, pp. 947-971, 2002.

[66] G. Wei, Y. Zhao, and Y. Xiang, "The determination of natural frequencies of rectangular plates with mixed boundary conditions by discrete singular convolution," *International Journal of Mechanical Sciences,* vol. 43, no. 8, pp. 1731-1746, 2001.

[67] Y. Zhao and G. Wei, "DSC analysis of rectangular plates with non-uniform boundary conditions," *Journal of Sound and Vibration,* vol. 255, no. 2, pp. 203-228, 2002.

[68] S. Yu, Y. Xiang, and G. Wei, "Matched interface and boundary (MIB) method for the vibration analysis of plates," *International Journal for Numerical Methods in Biomedical Engineering,* vol. 25, no. 9, pp. 923-950, 2009.

[69] S. Zhao, G. Wei, and Y. Xiang, "DSC analysis of free-edged beams by an iteratively matched boundary method," *Journal of Sound and Vibration,* vol. 284, no. 1-2, pp. 487-493, 2005.

[70] A. W. Leissa, "The free vibration of rectangular plates," *Journal of Sound and vibration,* vol. 31, no. 3, pp. 257-293, 1973.

[71] S. Eftekhari and A. A. Jafari, "High accuracy mixed finite element-Ritz formulation for free vibration analysis of plates with general boundary conditions," *Applied Mathematics and Computation,* vol. 219, no. 3, pp. 1312-1344, 2012.

[72] G. Karami and P. Malekzadeh, "Application of a new differential quadrature methodology for free vibration analysis of plates," *International Journal for Numerical Methods in Engineering,* vol. 56, no. 6, pp. 847-868, 2003.

[73] A. W. Leissa and Y. Narita, "Vibrations of completely free shallow shells of rectangular planform," *Journal of Sound and Vibration,* vol. 96, no. 2, pp. 207-218, 1984.

[74] D. Gorman, "Free vibration analysis of the completely free rectangular plate by the method of superposition," *Journal of Sound and Vibration,* vol. 57, no. 3, pp. 437-447, 1978.

[75] Y. Wang, X. Wang, and Y. Zhou, "Static and free vibration analyses of rectangular plates by the new version of the differential quadrature element method," *International Journal for Numerical Methods in Engineering,* vol. 59, no. 9, pp. 1207-1226, 2004.

[76] S. Soni, N. Jain, and P. Joshi, "Vibration analysis of partially cracked plate submerged in fluid," *Journal of Sound and Vibration,* vol. 412, pp. 28-57, 2018.

[77] X. Wang, "Free vibration analysis of angle-ply symmetric laminated plates with free boundary conditions by the discrete singular convolution," *Composite Structures,* vol. 170, pp. 91-102, 2017.

Appendix A

For the isotropic rectangular plate, the bending moments, equivalent shear forces and corner forces in a non-dimensional form are expressed as,

- Bending moments (M_X and M_Y):

$$M_X = D\left(\frac{\partial^2 W}{\partial X^2} + v\frac{\partial^2 W}{\partial Y^2}\lambda^2\right) \quad (\text{at } X = 0 \text{ and } X = L_1)$$
$$M_Y = D\left(\frac{\partial^2 W}{\partial Y^2}\lambda^2 + v\frac{\partial^2 W}{\partial X^2}\right) \quad (\text{at } Y = 0 \text{ and } Y = L_2) \tag{A1}$$

- Shear forces (Q_X and Q_Y):

$$Q_X = D\left[\frac{\partial^3 W}{\partial X^3} + (2-v)\frac{\partial^3 W}{\partial X \partial Y^2}\lambda^2\right] \quad (\text{at } X = 0 \text{ and } X = L_1)$$
$$Q_Y = D\left[\frac{\partial^3 W}{\partial Y^3} + (2-v)\frac{\partial^3 W}{\partial X^2 \partial Y}\lambda\right] \quad (\text{at } Y = 0 \text{ and } Y = L_2) \tag{A2}$$

- Corner force (R):

$$R = 2D(1-v)\frac{\partial^2 W}{\partial X \partial Y}\lambda \quad (\text{at each corner point of the plate}) \tag{A3}$$

While for the orthotropic rectangular plate, the bending moments, equivalent shear forces and corner forces are presented as,

- Bending moments (M_X and M_Y):

$$M_X = D_x\left(\frac{\partial^2 W}{\partial X^2} + v_y\frac{\partial^2 W}{\partial Y^2}\lambda^2\right) \quad (\text{at } X = 0 \text{ and } X = L_1)$$
$$M_Y = D_y\left(\frac{\partial^2 W}{\partial Y^2}\lambda^2 + v_x\frac{\partial^2 W}{\partial X^2}\right) \quad (\text{at } Y = 0 \text{ and } Y = L_2) \tag{A4}$$

- Shear forces (Q_X and Q_Y):

$$Q_X = D_x\left[\frac{\partial^3 W}{\partial X^3} + \left(v_y + \frac{G_{XY}h^3}{3D_X}\right)\frac{\partial^3 W}{\partial X \partial Y^2}\lambda^2\right] \quad (\text{at } X = 0 \text{ and } X = L_1) \tag{A5}$$

$$Q_Y = D_y \left[\frac{\partial^3 W}{\partial Y^3} \lambda^3 + \left(v_x + \frac{G_{XY} h^3}{3 D_Y} \right) \frac{\partial^3 W}{\partial X^2 \partial Y} \lambda \right] \quad \text{(at } Y = 0 \text{ and } Y = L_2\text{)}$$

- Corner force (R):

$$R = \frac{G_{XY} h^3}{3} \frac{\partial^2 W}{\partial X \partial Y} \lambda \quad \text{(at each corner point of the plate)} \qquad \text{(A6)}$$

Captions of Figures

Fig. 1. Geometry and coordinate system of a rectangular plate with surface part through cracks at the center.

Fig. 2. A line-spring model for a cracked plate with tensile stress and bending stress [7].

Fig. 3. Geometry and coordinate system of a bi-directionally restrained rectangular plate subjected to thermal loads [61].

Fig. 4. Cracked rectangular orthotropic plates with uni-directional in-plane restraints under thermal loads: (a) SS*SS* plate; (b) S*SS*S plate.

Fig. 5. Sketch of a rectangular plate with uniform points ($N = 7$, $M = 4$).

Fig. 6. Convergence study of non-dimensional frequency parameters for CCCC square plates.

Fig. 7. First four mode shapes for SSSS plates with a surface crack.

Fig. 8. First four mode shapes for CCCC plates with a surface crack.

Fig. 9. Effect of crack length on the fundamental frequency: (a) SFFF plate ($\lambda = 1$); (b) SCFF plate ($\lambda = 1$).

Fig. 10. Variation of critical buckling temperature with various crack length ratios for the simply supported isotropic plate and orthotropic plate ($L_1 = L_2 = 1$m): (a) $L_c' = 2a / L_1$; (b) $L_c' = 2b / L_2$.

Fig. 11. Variation of critical buckling temperature with various crack length ratios and directions for: (a) SS*SS* orthotropic plate ($L_1 = L_2 = 1$m); (b) S*SS*S orthotropic plate ($L_1 = L_2 = 1$m).

Fig. 12. Effect of temperature on the fundamental frequency: (a) intact plate ($L_1 = L_2 = 1$ m, $L_c' = 0$, $T_{cr} = 14.525$ °C); (b) cracked plate ($L_1 = L_2 = 1$ m, $L_c' = 2a / L_1 = 0.02$, $T_{cr} = 14.263$ °C).

Captions of Tables

Table 1 Comparison of frequency parameters Ω for SSSS intact isotropic plates (v = 0.3).

Table 2 Comparison of frequency parameters Ω for CCCC intact isotropic plates (v = 0.3).

Table 3 Comparison of frequency parameters Ω for FFFF intact isotropic plates (v = 0.3).

Table 4 Non-dimensional natural frequency Ω for cracked isotropic plates (v = 0.3, λ = 1).

Table 5 Non-dimensional natural frequency Ω for cracked isotropic plates (v = 0.3, λ = 1).

Table 6 Comparison of fundamental frequency parameters Ω for intact orthotropic plates (E_x/E_y = 2.45, v_x = 0.23, λ = 1).

Table 7 Properties of thin isotropic rectangular plates.

Table 8 Properties of thin orthotropic rectangular plates.

Table 9 Critical buckling temperature (°C) for intact and cracked SSSS plates (L_1 = L_2 = 1m).

Table 10 Fundamental frequency parameters Ω for cracked SSSS orthotropic plates (v_x = 0.23, v_y = 0.0208).

Table 11 Fundamental frequency parameters Ω for cracked SSSS isotropic plates in thermal environment (v = 0.33, L_1 = L_2 = 1 m).

Table 12 Fundamental frequency parameters Ω for cracked SSSS orthotropic plates in thermal environment (v_x = 0.23, v_y = 0.0208, L_1 = L_2 = 1 m).

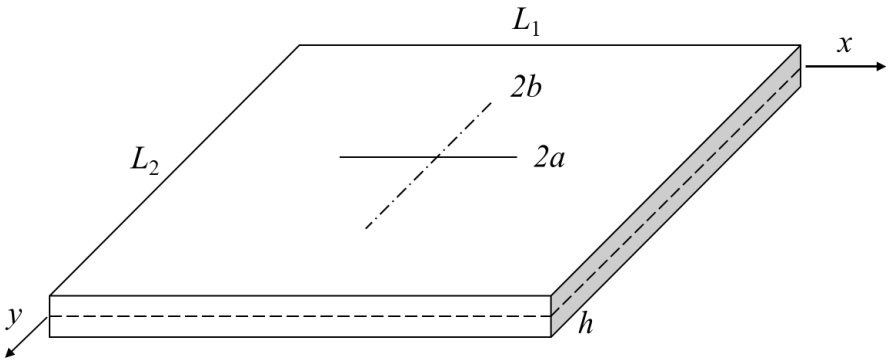

Fig. 1. Geometry and coordinate system of a rectangular plate with surface part through cracks at the center.

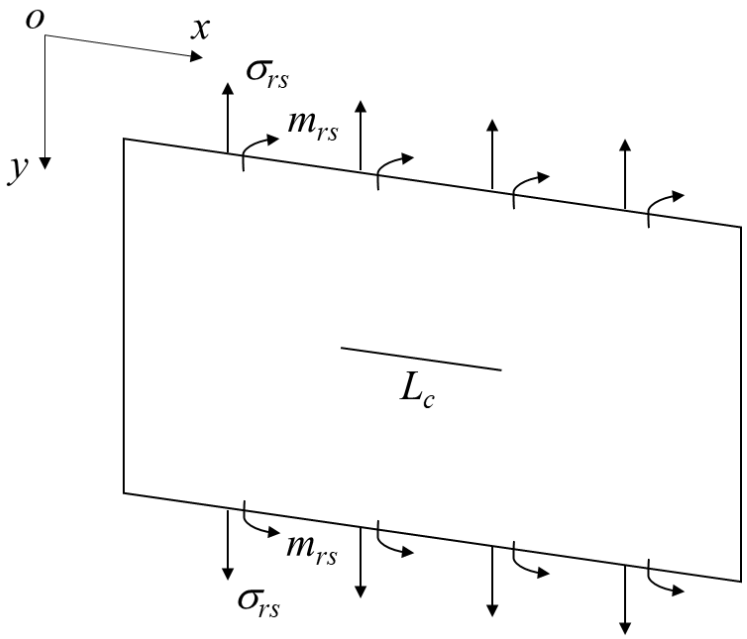

Fig. 2. A line-spring model for a cracked plate with tensile stress and bending stress [7].

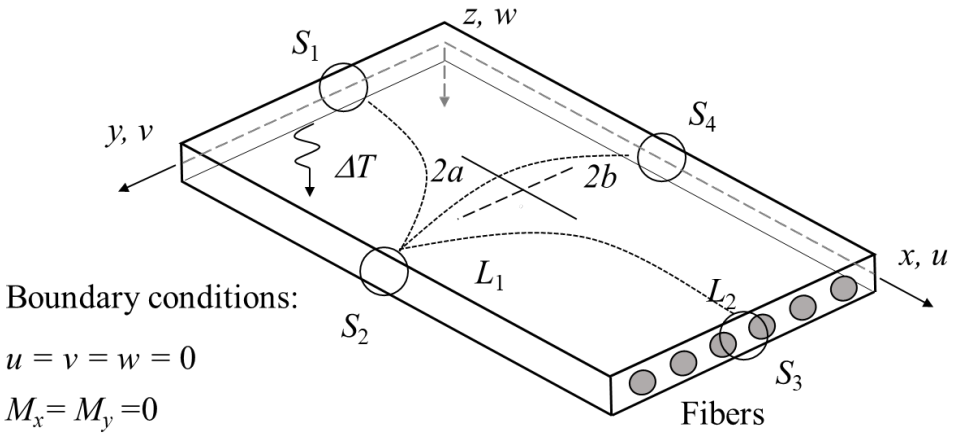

Fig. 3. Geometry and coordinate system of a bi-directionally restrained rectangular plate subjected to thermal loads [61].

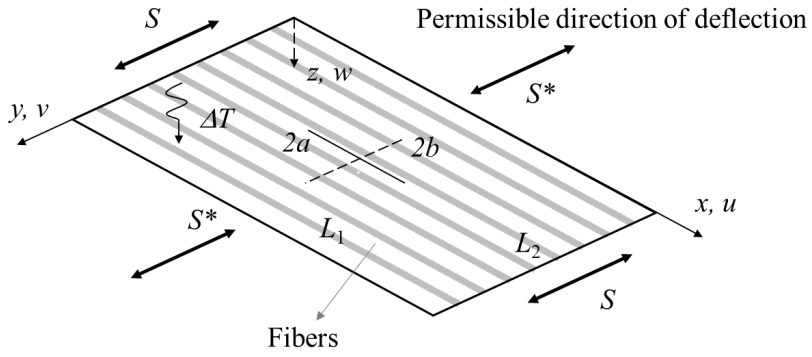

(a)

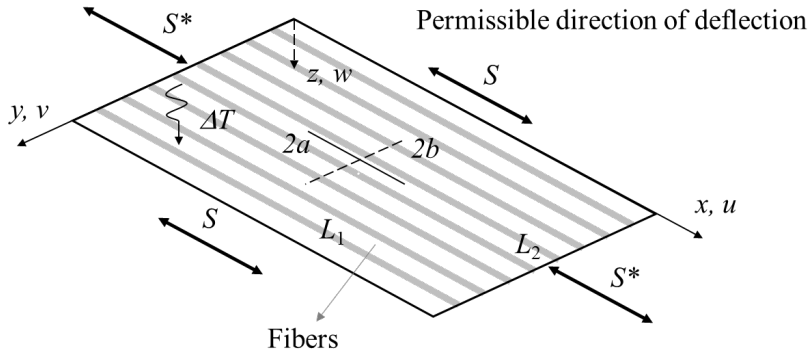

(b)

Fig. 4. Cracked rectangular orthotropic plates with uni-directional in-plane restraints under thermal loads: (a) SS*SS* plate; (b) S*SS*S plate.

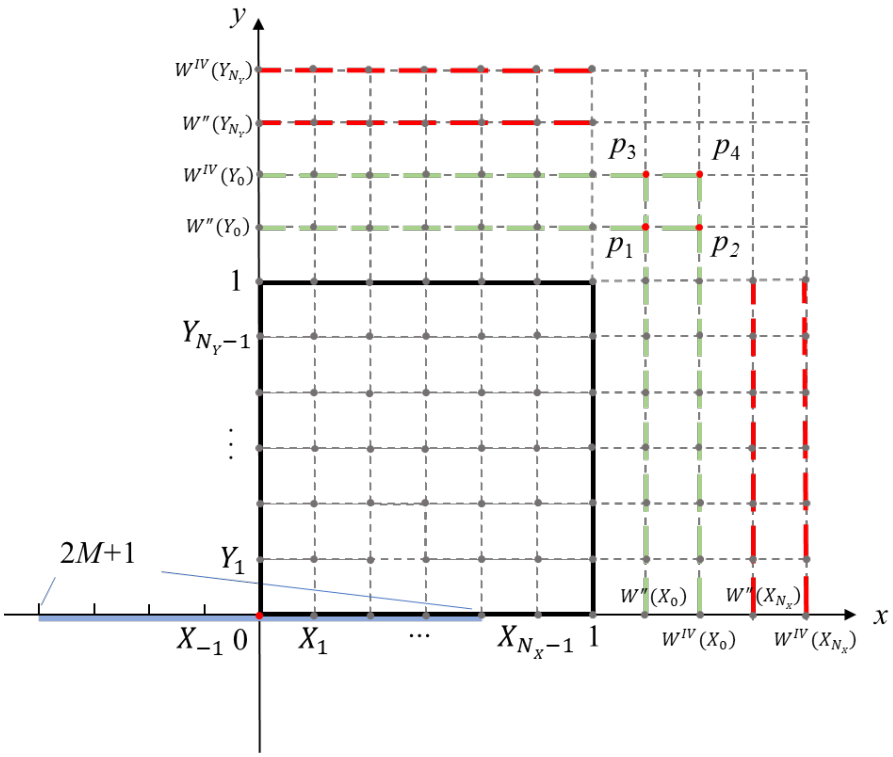

Fig. 5. Sketch of a rectangular plate with uniform points ($N = 7$, $M = 4$).

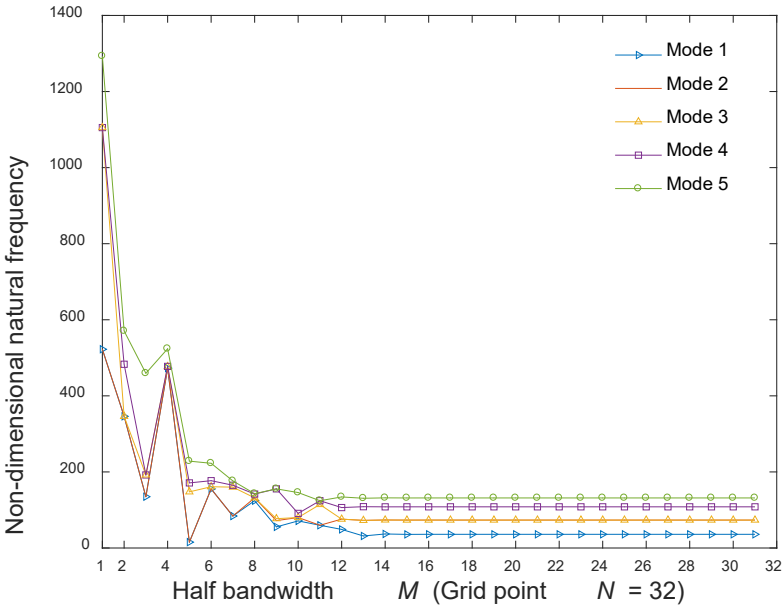

Fig. 6. Convergence study of non-dimensional frequency parameters for CCCC square plates.

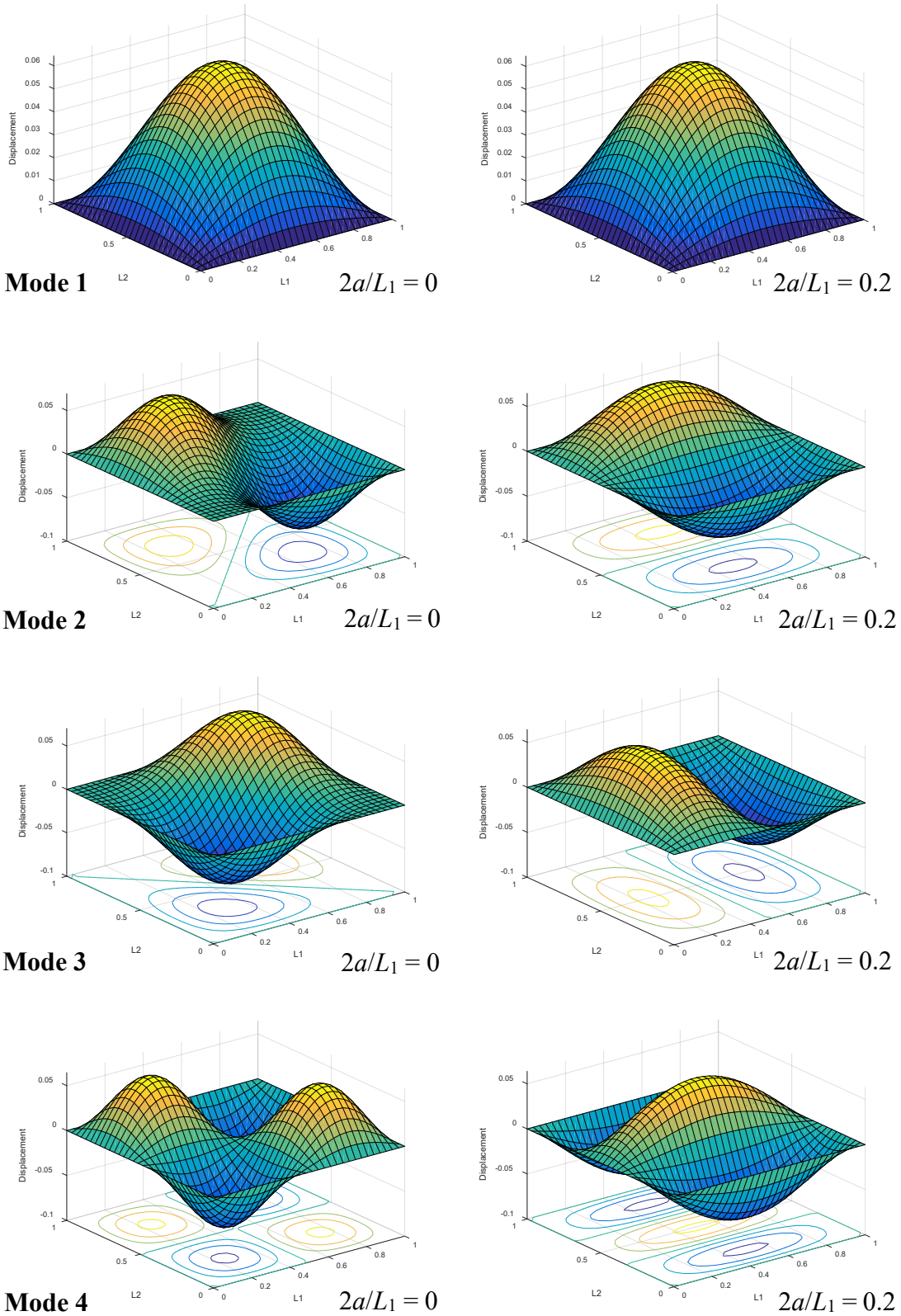

Fig. 7. First four mode shapes for SSSS plates with a surface crack.

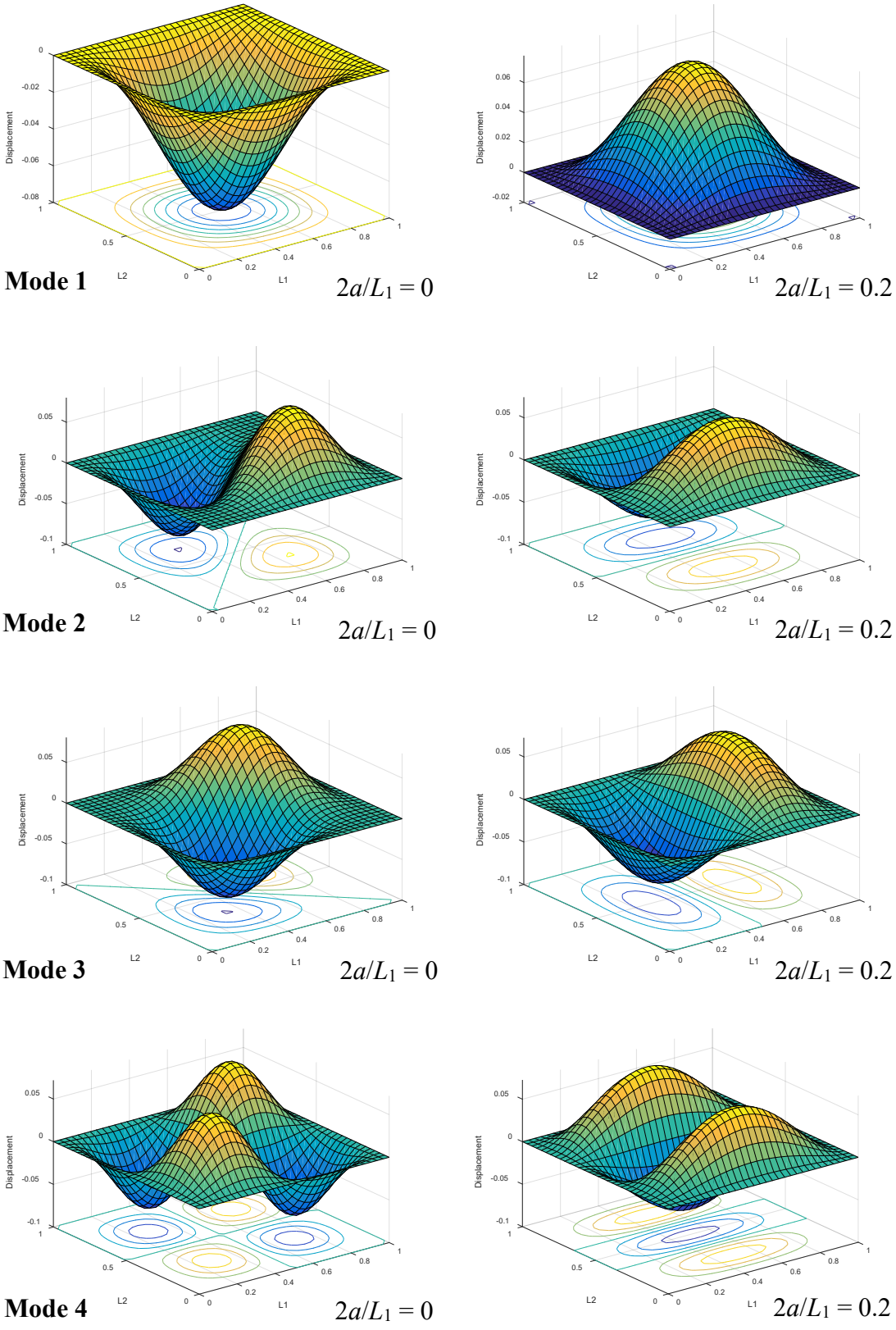

Fig. 8. First four mode shapes for CCCC plates with a surface crack.

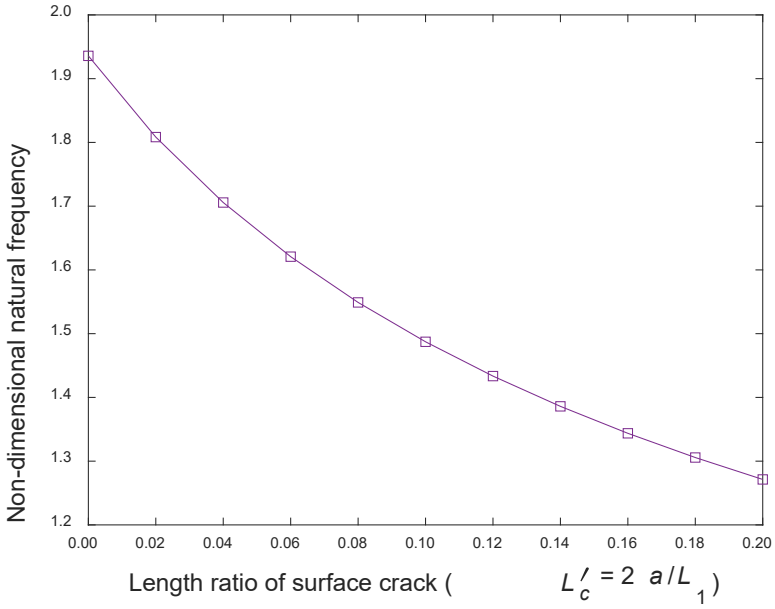

(a)

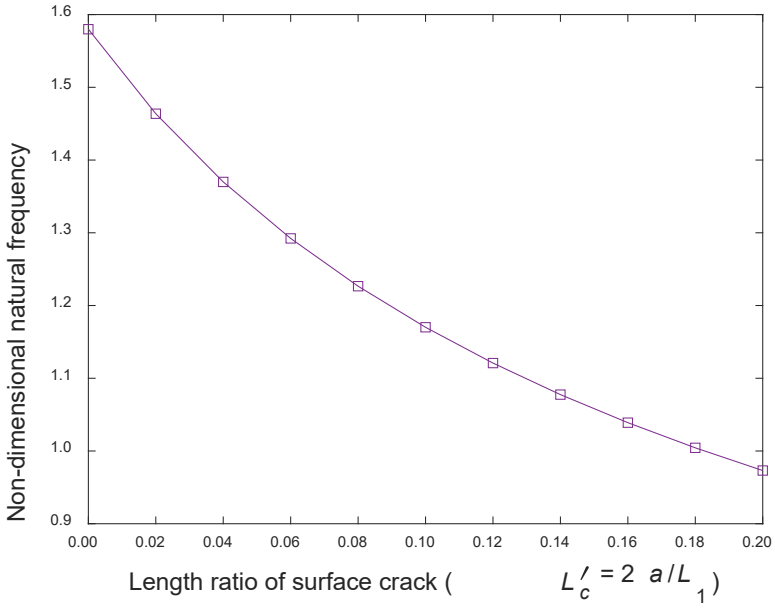

(b)

Fig. 9. Effect of crack length on the fundamental frequency:

(a) SFFF plate (λ = 1); (b) SCFF plate (λ = 1).

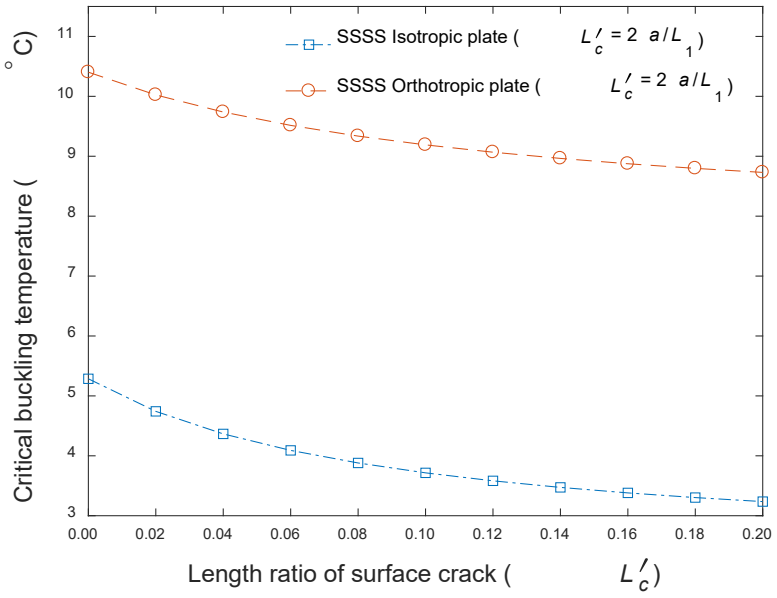

(a)

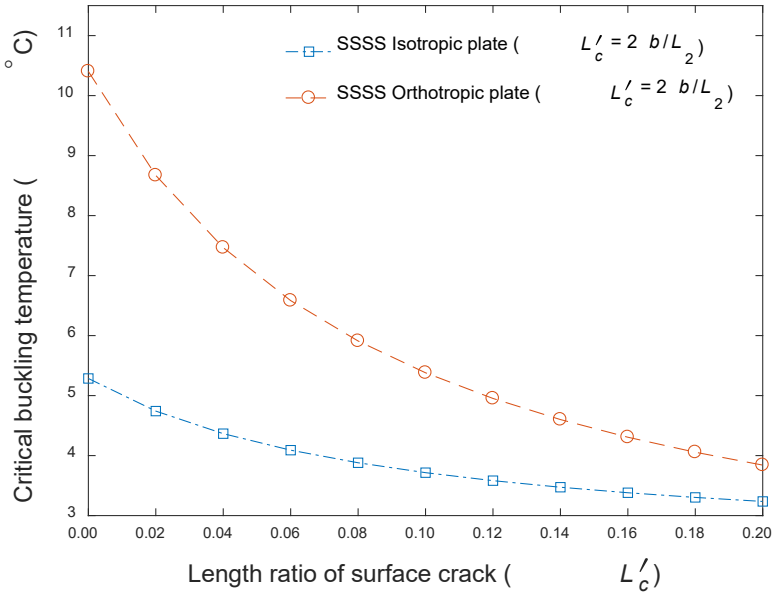

(b)

Fig. 10. Variation of critical buckling temperature with various crack length ratios for simply supported isotropic plate and orthotropic plate ($L_1 = L_2 = 1$ m):

(a) $L_c' = 2a / L_1$; (b) $L_c' = 2b / L_2$.

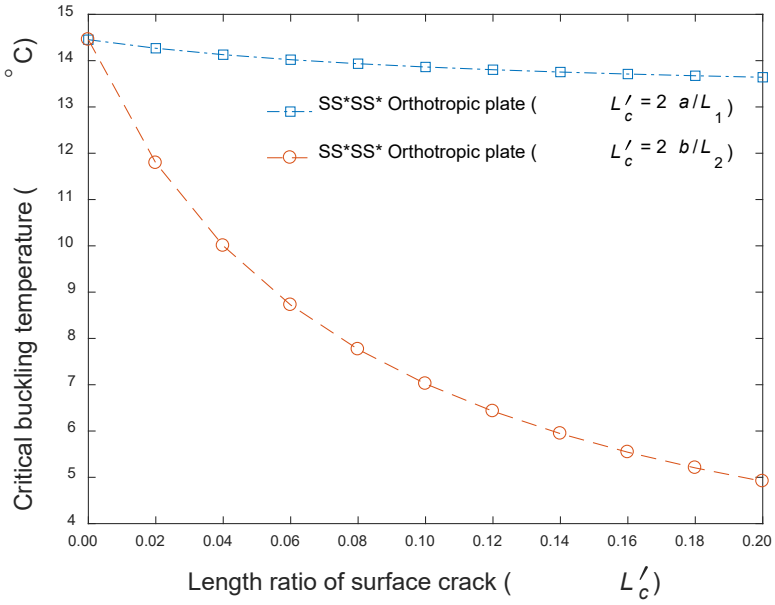

(a)

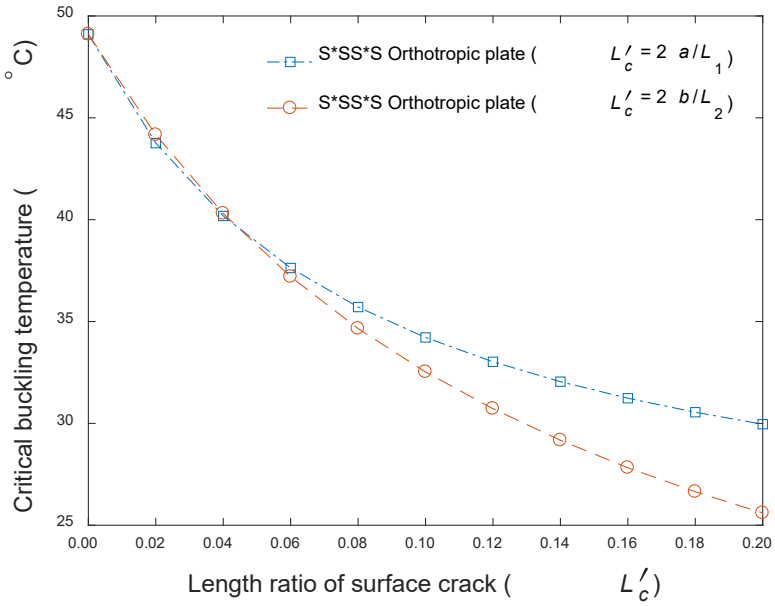

(b)

Fig. 11. Variation of critical buckling temperature with various crack length ratios and directions for: (a) SS*SS* orthotropic plate ($L_1 = L_2 = 1$ m); (b) S*SS*S orthotropic plate ($L_1 = L_2 = 1$ m).

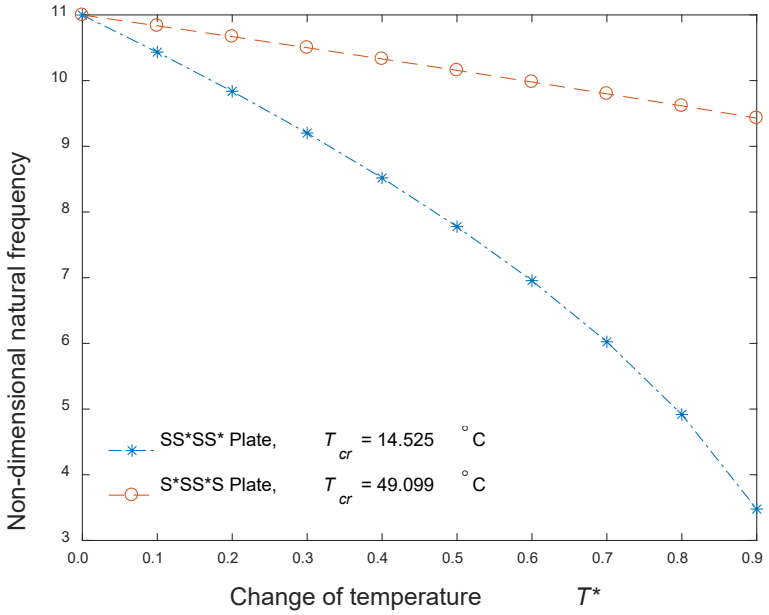

(a)

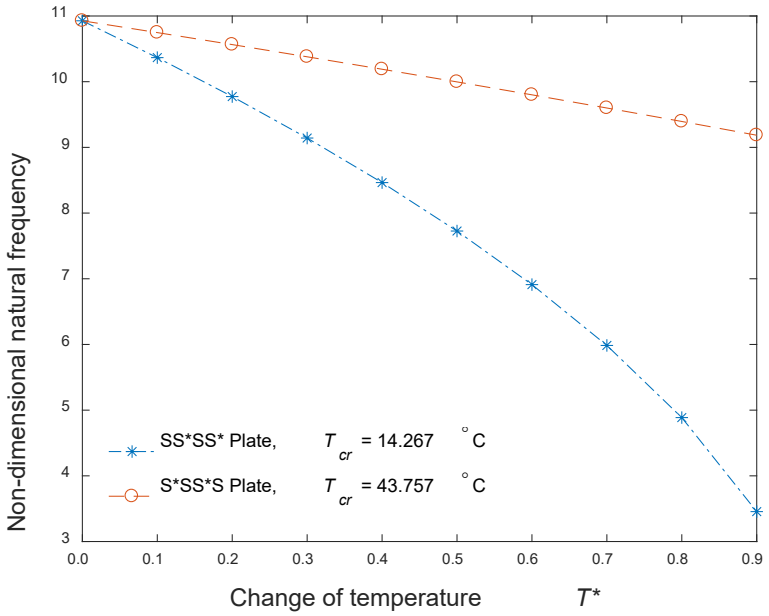

(b)

Fig. 12. Effect of temperature on the fundamental frequency:

(a) intact plate ($L_1 = L_2 = 1$ m, $L_c' = 0$, $T_{cr} = 14.525$ °C);

(b) cracked plate ($L_1 = L_2 = 1$ m, $L_c' = 2a / L_1 = 0.02$, $T_{cr} = 14.263$ °C).

Table 1
Comparison of frequency parameters Ω for SSSS intact isotropic plates (v = 0.3).

Mode sequence	Aspect ratio (λ = 1)		Aspect ratio (λ = 1.5)	
	Present work	Leissa [70]	Present work	Leissa [70]
1	19.739	19.739	32.076	32.076
2	49.348	49.348	61.685	61.685
3	49.348	49.348	98.696	98.696
4	78.957	78.957	111.033	111.033
5	98.696	98.696	128.305	128.305

Table 2
Comparison of frequency parameters Ω for CCCC intact isotropic plates (v = 0.3).

Mode sequence	Aspect ratio (λ = 1)			Aspect ratio (λ = 1.5)		
	Present work	Leissa [70]	Other methods	Present work	Leissa [70]	Other methods
1	35.987	35.992	35.9852[a]	60.764	60.772	60.7611[a]
2	73.401	73.413	73.394[b]	93.843	93.860	-
3	73.401	73.413	73.394[c]	148.793	148.820	-
4	108.234	108.270	108.210[b]	149.670	149.740	-
5	131.603	131.640	131.580[c]	179.586	179.660	-

[a] Based on the differential quadrature methodology [72].
[b] Based on the generalized differential quadrature method [38].
[c] Based on the mixed finite element-Ritz method [71].

Table 3
Comparison of frequency parameters Ω for FFFF intact isotropic plates (v = 0.3).

Mode sequence	Aspect ratio (λ = 1)			
	Present work	Leissa and Narita [73]	Gorman [74]	Wang *et al*. [75]
1	13.467	13.466	13.468	13.468
2	19.560	19.595	19.596	19.596
3	24.267	24.270	24.272	24.270
4	34.798	34.800	34.800	34.801
5	34.798	34.800	34.800	34.801

Table 4

Non-dimensional natural frequency Ω for cracked isotropic plates (v = 0.3, λ = 1).

Mode sequence	Crack length ratio ($2a/L_1$)	SSSS		CCCC	
		Present work	Soni *et al.* [76]	Present work	Soni *et al.* [76]
1	0.00	19.739	19.739	35.987	36.107
	0.02	19.247	19.247	34.816	34.944
	0.10	18.164	18.163	32.190	32.346
	0.20	17.564	17.563	30.695	30.884
2	0.00	49.348	49.348	73.401	73.737
	0.02	46.707	46.706	69.189	69.537
	0.10	40.562	40.560	59.297	59.694
	0.20	36.900	36.897	53.312	53.764
3	0.00	49.348	49.348	73.401	73.737
	0.02	49.018	49.018	72.685	73.045
	0.10	48.313	48.313	71.120	71.561
	0.20	47.936	47.936	70.244	70.763

Table 5

Non-dimensional natural frequency Ω for cracked isotropic plates ($v = 0.3,\ \lambda = 1$).

Mode sequence	Crack length ratio ($2a/L_1$)	SSFF		Crack length ratio ($2a/L_1$)	SCFF	
		Present work	Leissa [70]		Present work	Leissa [70]
1	0.00	3.3668	3.3687	0.00	5.3510	5.3639
	0.02	3.1663	-	0.02	4.9309	-
	0.10	2.6849	-	0.10	3.9059	-
	0.20	2.3784	-	0.20	3.2482	-
2	0.00	17.316	17.407	0.00	19.075	19.171
	0.02	16.484	-	0.02	18.535	-
	0.10	13.931	-	0.10	17.023	-
	0.20	12.177	-	0.20	15.330	-
3	0.00	19.292	19.367	0.00	24.671	24.768
	0.02	18.554	-	0.02	22.964	-
	0.10	17.289	-	0.10	19.043	-
	0.20	16.579	-	0.20	17.250	-

Table 6

Comparison of fundamental frequency parameters Ω for intact orthotropic plates (E_x/E_y = 2.45, v_x = 0.23, λ = 1).

Plate	Method	Mode number							
		1	2	3	4	5	6	7	8
SSSS	Present	15.170	33.248	44.387	60.681	64.456	90.144	93.630	108.458
	DQM [77]	15.171	33.248	44.387	60.682	64.457	90.145	93.631	108.460
CFCF	Present	22.333	24.684	34.324	55.925	61.580	64.808	75.806	91.303
	DQM [77]	22.331	24.682	34.323	55.924	61.574	64.801	75.799	91.301
SFFF	Present	4.965	15.203	17.545	21.482	37.020	42.010	49.845	55.486
	DQM [77]	4.966	15.202	17.546	21.484	37.023	42.010	49.845	55.487
CFFF	Present	3.507	6.878	18.376	22.067	27.337	42.046	42.689	61.560
	DQM [77]	3.507	6.879	18.377	22.067	27.337	42.048	42.670	61.558
FFFF	Present	9.982	14.120	22.379	24.669	29.860	39.387	48.551	49.298
	DQM [77]	9.984	14.119	22.379	24.671	29.862	39.387	48.556	49.301

Table 7

Properties of thin isotropic rectangular plates.

v	ρ (kg/m^3)	h (m)	E (GPa)	α (/°C)
0.33	2660	0.01	70.3	2.34×10^{-5}

Table 8

Properties of thin orthotropic rectangular plates.

v_x	v_y	h (m)	ρ (kg/m^3)	E_x (GPa)	E_y (GPa)	G_{xy} (GPa)	α_x (/°C)	α_y (/°C)
0.23	0.0208	0.01	2000	208	19.8	5.7	7.1×10^{-6}	2.3×10^{-5}

Table 9
Critical buckling temperature (°C) for intact and cracked SSSS plates ($L_1 = L_2 = 1$m).

Crack length ratio ($2a/L_1$)	Isotropic plate		Orthotropic plate	
	Present	Joshi *et al.* [33]	Present	Joshi *et al.* [33]
0.00	5.285	5.28	10.403	10.51
0.02	4.719	4.67	10.024	10.07
0.20	3.246	3.15	8.730	8.72

Table 10
Fundamental frequency parameters Ω for cracked SSSS orthotropic plates ($v_x = 0.23$, $v_y = 0.0208$).

Crack length ratio ($2a/L_1$)	Aspect ratio ($\lambda = 1$)		Crack length ratio ($2a/L_1$)	Aspect ratio ($\lambda = 2$)	
	Present work	Joshi *et al.* [33]		Present work	Joshi *et al.* [33]
0.00	10.998	10.99	0.00	17.256	17.25
0.02	10.927	10.91	0.02	16.628	16.54
0.10	10.771	10.75	0.10	15.163	14.98
0.20	10.685	10.66	0.20	14.296	14.11
0.40	10.611	10.59	0.40	13.518	13.37
0.60	10.578	10.56	0.60	13.157	13.04
0.80	10.559	10.54	0.80	12.948	12.85
1.00	10.547	10.53	1.00	12.812	12.73

Table 11

Fundamental frequency parameters Ω for cracked SSSS isotropic plates in thermal environment ($\nu = 0.33$, $L_1 = L_2 = 1$ m).

Temperature variation (T^*)	Crack length ratio ($2a/L_1 = 0$)		Crack length ratio ($2a/L_1 = 0.02$)	
	Present work	Joshi *et al.* [33]	Present work	Joshi *et al.* [33]
0	19.739	19.739	19.221	19.153
0.1	18.726	18.726	18.234	18.170
0.2	17.655	18.655	17.192	17.131
0.3	16.515	16.515	16.081	16.025
0.4	15.290	15.290	14.888	14.836
0.5	13.958	13.958	13.591	13.544
0.6	12.485	12.484	12.156	12.114
0.7	10.812	10.812	10.528	10.491
0.8	8.8276	8.8276	8.5958	8.5656
0.9	6.2421	6.2426	6.0781	6.0568

Table 12
Fundamental frequency parameters Ω for cracked SSSS orthotropic plates in thermal environment (v_x = 0.23, v_y = 0.0208, $L_1 = L_2$ = 1 m).

Temperature variation (T*)	Crack length ratio ($2a/L_1$ = 0)		Crack length ratio ($2a/L_1$ = 0.02)	Crack length ratio ($2b/L_2$ = 0.02)	
	Present work	Joshi *et al.* [33]	Present work	Present work	Joshi *et al.* [33]
0	10.998	10.998	10.927	10.430	10.352
0.1	10.434	10.433	10.366	9.9120	9.8431
0.2	9.8367	9.8366	9.7735	9.3653	9.3064
0.3	9.2013	9.2013	9.1422	8.7846	8.7371
0.4	8.5188	8.5188	8.4641	8.1626	8.1278
0.5	7.7764	7.7764	7.7266	7.4892	7.4690
0.6	6.9556	6.9556	6.9109	6.7489	6.7459
0.7	6.0237	6.0237	5.9850	5.9167	5.9356
0.8	4.9184	4.9184	4.8867	4.9465	4.9956
0.9	3.4778	3.4778	3.4554	3.7320	3.8316